Computers in Biology and Medicine 157 (2023) 106719

Contents lists available at ScienceDirect

Computers in Biology and Medicine

journal homepage: www.elsevier.com/locate/compbiomed

Steady-state and transient effects of SK channel block and adrenergic stimulation to counteract acetylcholine-induced arrhythmogenic effects in the human atria: A computational study

Chiara Celotto [a,b,*], Carlos Sánchez [a,b], Konstantinos A. Mountris [c], Pablo Laguna [a,b], Esther Pueyo [a,b]

[a] BSICoS Group, I3A and IIS-Aragón, University of Zaragoza, Spain
[b] CIBER - Bioingeniería, Biomateriales, y Nanomedicina (CIBER-BBN), Zaragoza, Spain
[c] Mechanical Engineering, University College London, London, United Kingdom

ARTICLE INFO

Keywords:
Atrial fibrillation
Autonomic nervous system
Acetylcholine
Small-conductance calcium-activated potassium channels
Isoproterenol

ABSTRACT

Hyperactivity of the parasympathetic nervous system has been linked to the development of paroxysmal atrial fibrillation (AF). The parasympathetic neurotransmitter acetylcholine (ACh) causes a reduction in action potential (AP) duration (APD) and an increase in resting membrane potential (RMP), both of which contribute to enhance the risk for reentry. Research suggests that small-conductance calcium activated potassium (SK) channels may be an effective target for treating AF. Therapies targeting the autonomic nervous system, either alone or in combination with other drugs, have been explored and have been shown to decrease the incidence of atrial arrhythmias. This study uses computational modeling and simulation to examine the impact of SK channel block (SKb) and β-adrenergic stimulation through Isoproterenol (Iso) on countering the negative effects of cholinergic activity in human atrial cell and 2D tissue models. The steady-state effects of Iso and/or SKb on AP shape, APD at 90% repolarization (APD_{90}) and RMP were evaluated. The ability to terminate stable rotational activity in cholinergically-stimulated 2D tissue models of AF was also investigated. A range of SKb and Iso application kinetics, which reflect varying drug binding rates, were taken into consideration. The results showed that SKb alone prolonged APD_{90} and was able to stop sustained rotors in the presence of ACh concentrations up to 0.01 μM. Iso terminated rotors under all tested ACh concentrations, but resulted in highly-variable steady-state outcomes depending on baseline AP morphology. Importantly, the combination of SKb and Iso resulted in greater APD_{90} prolongation and showed promising anti-arrhythmic potential by stopping stable rotors and preventing re-inducibility.

1. Introduction

Atrial fibrillation (AF) is a serious public health issue and a major contributor to rising healthcare expenses in Western countries [1]. Although it is not typically life-threatening, AF increases the risk of stroke three- to five-fold and can lead to heart failure. The pathophysiology of AF is highly complex and is defined based on a "pathophysiological triangle" that consists of triggers for arrhythmia initiation, a fibrotic substrate for its maintenance and numerous modulators [2]. Among these modulators, the autonomic nervous system (ANS) has been increasingly linked to the onset and perpetuation of AF [3–5]. Fluctuations in both the sympathetic and parasympathetic branches of the ANS have been shown to be involved in atrial tachyarrhythmias [6], with hyperactivity of the parasympathetic branch specifically associated with the onset of paroxysmal AF [7].

Postganglionic parasympathetic nerve fibers release the neurotransmitter acetylcholine (ACh) at their nerve endings, which binds to muscarinic receptors in atrial myocytes to activate a specific population of cardiac potassium channels (G protein-activated inwardly rectifying potassium channels). The resulting ACh-activated potassium current, I_{KACh}, causes shortening of the action potential (AP) duration (APD) and hyperpolarization of the resting membrane potential (RMP), with concentration-dependent effects. These ACh-induced effects contribute to a reduction in the wavelength of reentry (WL), which can facilitate reentrant activity by decreasing the distance covered by the depolarization wave during the effective refractory period (ERP). The heterogeneous spatial distribution of parasympathetic nerve endings and the rapid breakdown of ACh at its release site by acetylcholinesterase [4] make the effects of cholinergic stimulation on atrial

* Corresponding author.
E-mail address: chiaracelotto@unizar.es (C. Celotto).

https://doi.org/10.1016/j.compbiomed.2023.106719
Received 8 June 2022; Received in revised form 17 February 2023; Accepted 26 February 2023
Available online 5 March 2023

refractoriness highly heterogeneous, which enhances the susceptibility to AF occurrence and maintenance. Experimental and clinical studies have shown that certain cases of AF are sustained by high-frequency small reentrant sources called rotors [8].

Despite recent advancements in AF management, current pharmacological therapies still present limitations in terms of efficacy and side effects. Class III antiarrhythmic drugs target potassium channels driving AP repolarization, leading to an increase in APD and WL. To minimize potentially harmful side effects on the ventricles, potassium channels primarily expressed in the atria are being considered as targets for AF therapy.

Small-conductance calcium (Ca^{2+})–activated potassium (SK) channels have emerged as potential atrial-selective targets [4,9,10]. *In vivo* and *ex vivo* studies have postulated SK channel inhibition as a potential therapeutic strategy for AF treatment. By prolonging APD and ERP, SK channel inhibition may counteract the effects of parasympathetic stimulation in the atria [9,11].

In another line of research and based on the crucial role of the ANS in modulating atrial electrical activity, therapies targeting the ANS have been investigated and shown, applied individually or in combination with other treatments, to reduce the incidence of atrial arrhythmias [4]. In particular, some studies have explored the interaction between adrenergic and cholinergic stimulation effects in the atria. In [12], low concentrations of isoproterenol (Iso), a non-specific β-adrenergic agonist, were found to significantly counteract cholinergic effects by limiting the shortening of APD caused by ACh. This modulation of atrial repolarization is due to Iso's effects on the sarcoplasmic reticulum (SR), slow component (I_{Ks}) and ultrarapid component (I_{Kur}) of the delayed rectifier potassium current, and L-type calcium current (I_{CaL}), among others [13–16].

This study aims to evaluate the effectiveness of combining β-adrenergic stimulation and SKb in countering cholinergic-induced abnormalities in atrial electrical activity. Our hypothesis is that the simultaneous application of Iso and SKb can prolong the APD shortened by ACh and restore it to its baseline state. To test this hypothesis, numerical simulations are conducted using human atrial cell and 2D tissue models that consider adrenergic, cholinergic and SKb effects. The steady-state effects of Iso and/or SKb on AP shape and APD_{90} (APD at 90% repolarization) are evaluated. The efficacy of Iso and SKb, both individually and in combination, in terminating rotational activity in a cholinergically stimulated 2D tissue model of AF is also investigated. A range of SKb and Iso application kinetics, representative of different drug binding rates, are considered to assess the role of pharmacokinetics in rotor termination under varying levels of cholinergic activation.

2. Methods

2.1. Human atrial cell models

We took three previously published computational models of human atrial cellular electrophysiology as a basis for our research. These models were built based on different sets of human and animal experimental data and rely on slightly different formulations of ionic currents, pumps and exchangers. Thus, they differ in AP morphology and rate adaptation properties, which may reflect the inherent diversity in cell phenotypes of the human atria. To test the model independence of our findings, we selected a model of each of the three main types of available atrial cellular models in the literature: Courtemanche, Nygren-Maleckar-Koivumäki-Skibsbye and Grandi [17]. Specifically, we used the Courtemanche ($\mathcal{C}$) [18], Skibsbye ($\mathcal{S}$) [9], and Grandi ($\mathcal{G}$) [19] human atrial AP models. For each of the three models, the effects of cholinergic and adrenergic stimulation and the formulation of the I_{SK} current were incorporated, as described in the following sections, and are summarized in Table 1.

2.1.1. Cholinergic and β-adrenergic stimulation

The parasympathetic stimulation effects were described by introducing an ACh-activated potassium current (I_{KACh}) in the models to account for the activation of G protein-activated inwardly rectifying potassium channels induced by ACh. The I_{KACh} was defined differently in the three models, with the definition in the $\mathcal{C}$ model based on Kneller et al. [20] and updated as proposed by Bayer et al. [21]. In contrast, the $\mathcal{G}$ and $\mathcal{S}$ models adopted the formulation by Voigt et al. [22], with further adjustments in the $\mathcal{G}$ model based on the experimental data from Koumi et al. [19,23].

Sympathetic stimulation affects atrial myocytes by activating the β-adrenergic signaling cascade, which triggers the phosphorylation of various cellular substrates by protein kinase A (PKA). In the $\mathcal{C}$ and $\mathcal{S}$ models, the effects of β-adrenergic stimulation were modeled as proposed by González de la Fuente et al. [13]. This involved modeling the increases in the maximal conductances of I_{CaL} and I_{Ks}, and the decrease in the maximal conductance of the transient outward potassium current (I_{to}) following reported concentration-dependent conductance modulation curves [13]. At an Iso concentration of 1 μM, the maximal conductances of I_{CaL} and I_{Ks} were increased by 160.6% and 65.7%, respectively, while the maximal conductance of I_{to} was reduced by 18.6%.

In the $\mathcal{G}$ model, the effects of β-adrenergic stimulation were modeled based on the method described in [24]. This involved PKA regulation of various sub-cellular targets, such as a 3-fold increase in the maximal conductance of I_{Ks} and a 40 mV leftward shift in the IV relationship, a 3-fold increase in the maximal conductance of I_{Kur} and a 50% increase in the fraction of available channels for I_{CaL} with a 3 mV leftward shift in the channel availability. The sensitivity of the SR Ca^{2+} ATPase (SERCA) to Ca^{2+} was increased by reducing the forward mode k_{mf} by 50%. The sensitivity of the ryanodine receptors (RyR) to Ca^{2+} was increased 2-fold, while the troponin affinity for Ca^{2+} (TnI) was decreased by increasing k_d by 50%. Finally, the affinity of the Na^+/K^+ pump (I_{NaK}) for $[Na^+]_i$ was increased by 25% [19].

2.1.2. Human atrial SK current

For the $\mathcal{S}$ model, the description of the I_{SK} current was already included as per Skibsbye et al. [25]. For the $\mathcal{C}$ and $\mathcal{G}$ models, new descriptions of the I_{SK} current were introduced based on the formulations by Engel et al. [26] and Peñaranda et al. [27], respectively. These formulations were selected and adjusted to match the experimental I_{SK} characteristics found in the literature [9,28]. The conductance, g_{SK}, was modified so that complete inhibition of I_{SK} resulted in a 20% increase in APD_{90}, as observed in isolated atrial myocytes and atrial trabeculae strips from sinus rhythm patients [9,29]. In all subsequent analyses, the I_{SK} current was included as part of the baseline model.

2.1.3. AF-induced electrical remodeling

The human atrial cardiomyocyte models described in 2.1 were considered to represent atrial cells in either sinus rhythm or with early-onset AF. Models of persistent AF (psAF) were generated by incorporating AF-induced electrical remodeling. In the $\mathcal{C}$ model, electrical remodeling was simulated by reducing the maximal conductances of I_{to}, I_{CaL} and I_{Kur} by 50%, 70% and 50%, respectively, and by increasing the maximal conductance of the inward rectifier potassium current (I_{K1}) by 100% [30].

In the $\mathcal{G}$ model, electrical remodeling involved reductions in the conductivities of I_{to}, I_{Kur} and the fast sodium current (I_{Na}) by 45%, 45% and 10%, respectively. Additionally, a late component was added to the I_{Na} current, as previously described [31]. The density of I_{CaL} was reduced by 50%, sensitivity of the RyR to luminal Ca^{2+} was doubled, and the rate of the SERCA pump was decreased [32]. The conductivities of I_{K1}, I_{Ks} and the sodium–calcium exchange current (I_{NaCa}) were increased by 100%, 100% and 40%, respectively. Finally, passive SR calcium leak was increased by 25% [19].

Table 1
Summary of formulations for descriptions of cholinergic (ACh) and β-adrenergic modulation (1 μM Iso), SK current (I_{SK}) and psAF-induced electrical remodeling.

Models	ACh	Iso	I_{SK}	psAF
($\mathcal{C}$)	I_{KACh} as in *Kneller* [20] + *Bayer* [21]	I_{to}: −48.6% I_{CaL}: +160.6% I_{Ks}: +65.7% *González* [13]	I_{SK} as in *Engel* [26]	I_{to} −50% I_{CaL}: −70% I_{Kur}: −50% I_{K1}: −70% *Courtemanche* [18] g_{SK}: −50%
($\mathcal{G}$)	I_{KACh} as in *Voigt* [22]	I_{Ks}: enhanced maximal conductance (3-fold) and leftward shift in IV relationship (by 40 mV). g_{Kur}: enhanced 3-fold. I_{CaL}: increased fraction of available channels (+50%), and channel availability shifted leftward (by 3 mV). SERCA forward mode k_{mf}: reduced by 50%. RyR Sensitivity to Ca^{2+}: enhanced 2-fold. TnI: decreased (k_d increased by 50%). I_{NaK} affinity for $[Na^+]_i$: increased by 25%. *Grandi* [19]	I_{SK} as in Peñaranda [27]	I_{Na} −10% peak density. I_{NaL}: added late component. I_{Ks}: increased 2 fold. I_{Kur}: −45%. I_{K1}: upregulated 100%. I_{to}: −45%. I_{CaL}: current density is reduced by 50%. I_{NaCa}: upregulated in cAF (+40%). SERCA: reduced maximal pump rate. RyR: 2-fold increasing in sensitivity for luminal Ca. SR Ca^{2+} leak: increased by 25%. *Grandi* [19] g_{SK}: −50%
($\mathcal{S}$)	I_{KACh} as in *Voigt* [22]	I_{to}: −48.6% I_{CaL}: +160.6% I_{Ks}: +65.7% González [13]	I_{SK} as in *Skibsbye* [9]	g_{Na}: −18% g_{CaL}: −55% g_{to}: −62% g_{Kur}: −38% g_{Ks}: +145% g_{K1}: +68% g_{NaCa}: +50% PLB: +18% SLN: −40% Cell length: +10% SERCA expression: −18% RyR: +100% g_{SK}: −50% *Skibsbye* [9]

In the $\mathcal{S}$ model, under psAF-related electrical remodeling, I_{CaL}, I_{to}, I_{Kur}, I_{Na} and the sarcolipin to SERCA ratio (SLN) were reduced by 55%, 62%, 38%, 18%, and 40%, respectively, while I_{K1}, I_{Ks}, the sodium–calcium exchanger current (I_{NaCa}), and the phospholamban to SERCA ratio (PLB) were increased by 68%, 145%, 50% and 18%, respectively [9]. Additionally, the expression of SERCA was decreased and the sensitivity of RyR to SR calcium was increased 2-fold. Cell dilation was also considered by increasing the cell length by 10% [9].

Regarding I_{SK}, AF-induced remodeling was considered to reduce the magnitude of the I_{SK} current by 50% in all models, in concurrence with experimental evidence [9]. Finally, the Iso formulation from González et al. provided specific conductance modulation curves for the psAF case.

2.2. Human atrial tissue models

The effects of cholinergic and adrenergic stimulation and SKb were investigated by modeling 2D human atrial tissues of 5 × 5 cm^2. The models considered a longitudinal diffusion coefficient of 0.003 cm^2/ms and a transverse-to-longitudinal diffusion coefficient ratio of 0.5. The longitudinal conduction velocity was found to be 94.12 cm/s, which is in line with experimental data reported in the literature [21]. The analysis of steady-state electrophysiological properties considered both a homogeneous spatial distribution of ACh and a heterogeneous distribution with circular patches of 0.5-cm radius. For the analysis of transient electrophysiological properties, only a uniformly distributed ACh was considered. After verifying that the combination of SKb and Iso produced comparable results in all three analyzed AP models, tissue analysis was performed using only the $\mathcal{C}$ model.

2.3. Numerical simulations

Single cells were subjected to pacing with a fixed cycle length (CL) until they reached steady state in each of the three employed models. Steady state was considered achieved when changes in state variables between consecutive stimuli measured at the end of each cardiac cycle were smaller than 3%. In particular, the $\mathcal{C}$ model was paced for 10 min, while the $\mathcal{G}$ and $\mathcal{S}$ models were paced for 5 min.

The temporal evolution of the transmembrane potential in single cells was described by the ordinary differential equation:

$$\frac{dV(t)}{dt} = -\left(\frac{I_{ion}(t) + I_{stim}(t)}{C_m}\right) \quad (1)$$

where C_m represents the total membrane capacitance, I_{ion} is the sum of all transmembrane ionic currents and I_{stim} represents the external stimulus current.

The $\mathcal{C}$ model was used for tissue simulations with its state variables initialized to the steady-state values obtained from single cell simulations. The temporal resolution for the $\mathcal{S}$ and $\mathcal{C}$ models was 0.005 ms, while the $\mathcal{G}$ model was run with a temporal resolution of 0.001 ms, ensuring numerical convergence of the results. In the tissue simulations, a spatial resolution of 0.02 cm was considered.

The electrical propagation in the tissue was described using the monodomain reaction–diffusion equation:

$$\nabla \cdot (\mathbf{D}\nabla(t)) = \chi C_m \frac{dV(t)}{dt} + \chi I_{ion}(t) \quad (2)$$

where χ represents the cell's surface area-to-volume ratio, V is the transmembrane potential, I_{ion} is the sum of all transmembrane ionic currents, C_m is the membrane capacitance, and $\mathbf{D}$ is the conductivity tensor.

The cellular simulations were performed using MATLAB, while tissue simulations were performed using ELECTRA, an in-house software that implements the Finite Element Method (FEM) and Meshfree

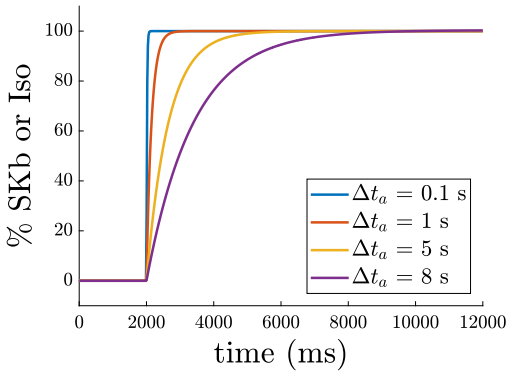

Fig. 1. Load curves for Iso and SKb expressed as percentage of SKb and Iso concentration with respect to 1 μM Iso and complete SKb, respectively.

Methods for the solution of the monodomain model [33–35]. In this work, FEM was used.

2.4. Analysis of steady-state and transient electrophysiological behavior

2.4.1. Steady-state behavior

At the cellular level, the impact of cholinergic stimulation on APs was studied at ACh concentrations of 0.001, 0.01, 0.1 and 1 μM. These ACh concentrations were within the ranges tested in previous studies [21]. In the tissue, the effects of ACh concentrations of 0.01 and 0.1 μM were investigated. The individual and combined effects of SKb and β-adrenergic stimulation were studied in conjunction with the various ACh levels. The impact of β-adrenergic stimulation was simulated by adding a saturating concentration of Iso of 1 μM, while the effect of complete SKb was simulated by reducing the conductance, g_{SK}, of the I_{SK} current to zero. SKb and Iso were applied uniformly throughout the tissue, regardless of whether ACh was distributed homogeneously or heterogeneously. To study the frequency-dependent effects, the models were paced at fixed CLs of 300, 500 and 1000 ms and AP properties were evaluated at steady state for each of those CL values.

2.4.2. Transient behavior

The tissue was subjected to a cross-stimulation protocol to induce reentrant activity, consisting of two stimuli, S1 and S2. S1 was delivered to the bottom edge of the tissue, while S2 was applied to a 2.5 x 2.5 cm^2 square at the bottom right corner. The timing of S2 was determined based on the concentration of ACh, as it altered the APD and conduction velocity. For ACh concentrations of 0.01 and 0.1 μM, the timing of S2 was equal to 155 and 105 ms, respectively. A rotor was considered stable if it did not end spontaneously during the 12-second simulation time. Once stability was confirmed, the simulation was restarted with the same initial conditions. After the first two seconds of simulation, 1 μM Iso and total SKb were progressively introduced following the load curves illustrated in Fig. 1 [36] to assess their ability to halt the initiated rotor. The load curves were defined to depict different drug association rates to evaluate whether rotor termination was affected by the application kinetics. The time intervals Δt_a to go from 0 to maximum (either Iso concentration or SKb) were equal to 0.1, 1, 5, and 8 s. The simulation was run for a total of 12 s. After a rotor was stopped, different S1-S2 intervals were applied again to the tissue to test for rotor re-inducibility, with the application time of the S1-S2 stimuli varying from 100 to 1000 ms after the rotor stopped.

3. Results

3.1. Human atrial cell

3.1.1. Individual cholinergic, β-adrenergic and SKb effects

Cholinergic stimulation with ACh had a concentration-dependent effect on RMP hyperpolarization and APD_{90} shortening in all three analyzed AP models, which aligns with previous experimental findings [12,29]. The shape of the AP was not significantly altered. The top row of Figs. 2 and 3 show the steady-state AP and APD_{90} at different ACh concentrations, with a cycle length (CL) of 1000 ms. Results for CLs of 500 and 300 ms can be found in the Supplementary Material (Fig. 1S).

ACh had a stronger effect on the $\mathcal{G}$ model compared to the $\mathcal{C}$ and $\mathcal{S}$ models. At the highest tested concentration of 0.1 μM, ACh reduced APD_{90} by 84.12% in the $\mathcal{G}$ model, 51.85% in the $\mathcal{C}$ model and 41.3% in the $\mathcal{S}$ model. Additionally, ACh decreased RMP by 6.32 mV in the $\mathcal{G}$ model, 5.50 mV in the $\mathcal{C}$ model and 2.37 mV in the $\mathcal{S}$ model. These results are presented in the first row of Fig. 2.

Iso stimulation with 1 μM had different effects on APD_{90} depending on the baseline AP morphology, as seen in the middle row of Fig. 2. In the $\mathcal{C}$ model, Iso shortened APD_{90} by 19.11%, whereas in the $\mathcal{G}$ and $\mathcal{S}$ models, Iso slightly prolonged APD_{90}. In the $\mathcal{C}$ model, Iso caused a strong plateau elevation and changed the AP from a triangular to a rectangular shape. This variation in AP response to Iso is consistent with previous research, with some studies observing APD_{90} shortening [12,37] and others observing APD_{90} prolongation [13,20,38].

The application of SKb led to a longer phase 3 of the AP due to a reduction in the outward potassium current. As a result, the APD_{90} was increased. The AP morphology was particularly affected in the $\mathcal{C}$ model, with a notable prolongation of the plateau phase, as shown in the middle row of Fig. 2.

When a concentration of 1 μM Iso and SKb were applied together, they acted synergistically to prolong the APD_{90} to values higher than those induced by SKb alone. The more pronounced effects of the combination of Iso and SKb were observed in the $\mathcal{C}$ model, with strong plateau elevation and prolongation, as seen in the middle row of Fig. 2.

The individual effects of ACh, Iso and SKb were compared with experimental results published in the literature, both qualitatively (Fig. 4) and quantitatively (Fig.2S in the Supplementary Material). Fig. 4 presents a qualitative comparison between the computed APs and experimental APs from various studies. It is worth noting that these experimental results were obtained from different animal species due to the scarcity of experimental data from humans.

3.1.2. Combined cholinergic, β-adrenergic and SKb effects

APs under cholinergic stimulation by 0.1 μM ACh, applied individually and in combination with β-adrenergic stimulation and/or I_{SK} block, are depicted in the bottom row of Fig. 2 for a constant CL of 1000 ms. A summary of the results in terms of APD_{90} is shown in Fig. 3. Results for CLs of 500 and 300 ms can be found in the Supplementary Material (Fig.3S).

SKb effectively neutralized the effects of cholinergic stimulation for ACh concentrations up to 0.001 μM in the $\mathcal{C}$ and $\mathcal{G}$ models and up to 0.01 μM in the $\mathcal{S}$ model. For the highest concentration of ACh (0.1 μM), SKb prolonged APD_{90} by 7.9% and 24.3% of the APD decrease caused by ACh in the $\mathcal{C}$ and $\mathcal{G}$ models, respectively, while its effects were negligible in the $\mathcal{S}$ model.

The effects of β-adrenergic stimulation applied on top of ACh were highly dependent on the baseline AP shape. A concentration of 1 μM Iso reduced the cholinergic-induced changes in the $\mathcal{G}$ and $\mathcal{S}$ models, but further shortened APD_{90} in the $\mathcal{C}$ model. In the $\mathcal{G}$ model, β-adrenergic effects weakened with increasing ACh concentrations, while in the $\mathcal{S}$ model, Iso effects grew proportionally with the increase in ACh concentration, recovering 71.6% of the APD_{90} change for the highest tested ACh concentration.

The combination of SK block and 1 μM Iso counteracted ACh effects in all cases, with the exception of the $\mathcal{G}$ model with the highest concentration of ACh (0.1 μM), in which the combination did not enhance the effect caused by Iso alone. For the $\mathcal{C}$ and $\mathcal{S}$ models, the combined action led to the recovery of baseline APD_{90}, with the prolongation being 45.23% and 83.5% of the APD_{90} shortening caused by 0.1 μM ACh, respectively. The above-described effects on APD_{90} were accompanied

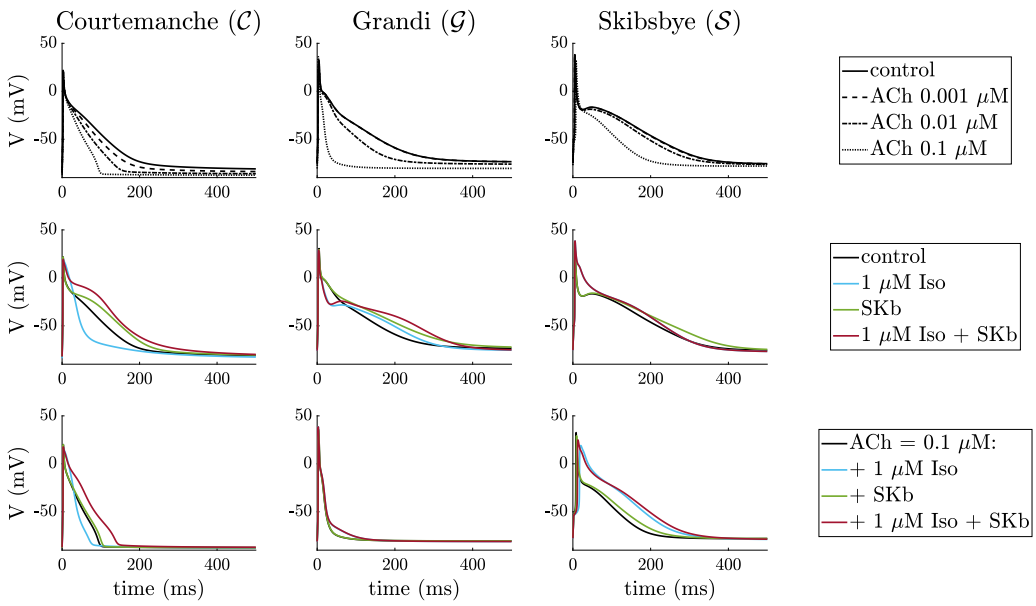

Fig. 2. APs of human atrial cardiomyocytes models paced at a CL of 1000 ms. First row: simulated effects of ACh (at concentrations of 0.001, 0.01 and 0.1 μM). Second row: Iso (at 1 μM concentration) and SKb. Third row: Iso (at 1 μM concentration) and SKb on top of 0.1 μM ACh.

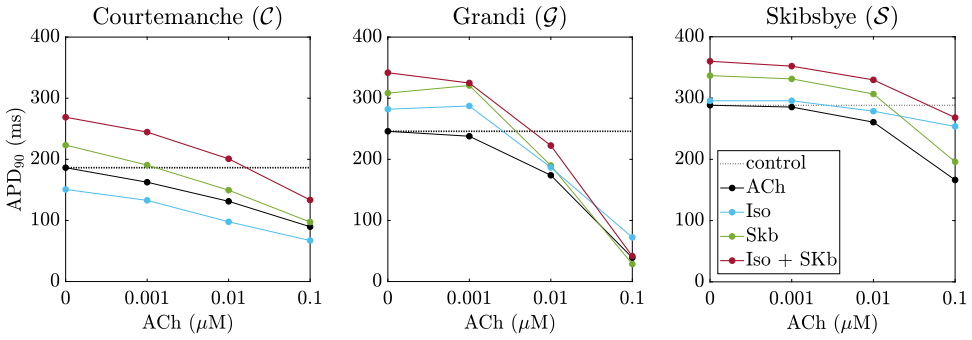

Fig. 3. APD_{90} vs. ACh concentration for human atrial myocytes models paced at a CL of 1000 ms at four different tested scenarios comprising cholinergic stimulation individually and in combination with β-adrenergic stimulation and/or SKb.

by changes in AP morphology for the $\mathcal{C}$ and $\mathcal{S}$ models, as evident from the bottom row of Fig. 2, where β-adrenergic stimulation and/or SKb applied on top of 1 μM ACh caused a significant elevation of the AP plateau.

3.1.3. Frequency-dependent effects

The dependence of APD_{90} shortening on pacing frequency, as a result of ACh, β-adrenergic and SKb effects, was analyzed by comparing the relative changes in the AP waveform and APD_{90} values at pacing CLs of 300, 500 and 1000 ms. The results for CL = 1000 ms are shown in Fig. 5, expressed as a percentage of the APD_{90} change relative to the control case. The results for CLs of 500 and 300 ms can be found in the Supplementary Material (Fig. 4S and 5S).

The relative ACh-induced APD_{90} shortening was largely independent of the CL in all models, with differences up to 3%, except when ACh was applied at 0.001 μM in the $\mathcal{S}$ model, where differences between the CLs of 1000 and 500 ms were of 13.45%.

The frequency dependence of APD_{90} changes induced by the application of 1 μM Iso on top of ACh was more pronounced, but it was reduced with increasing ACh concentration in the $\mathcal{C}$ and $\mathcal{G}$ models. In the $\mathcal{C}$ model, when Iso was applied on top of 0.001 μM ACh, it caused further shortening that increased, in relative terms, with reducing the CL. In the $\mathcal{G}$ model, Iso generally prolonged APD_{90} that was shortened by ACh, except when CL = 300 ms and ACh concentration = 0.001 μM ACh, where Iso further shortened it. In the $\mathcal{S}$ model, Iso strongly prolonged APD_{90} in all cases, except when pacing at 1000 ms and using 0.001 and 0.1 μM ACh, where APD_{90} was only slightly prolonged.

In the $\mathcal{S}$ and $\mathcal{C}$ models, SKb showed little frequency dependence, while in the $\mathcal{G}$ model, SKb showed mild frequency dependence that decreased with increasing ACh concentration and was stronger for lower pacing frequencies.

The combination of Iso and SKb applied on top of ACh showed weak frequency dependence in the $\mathcal{C}$ model, while in the $\mathcal{G}$ model, it presented stronger effects for lower pacing frequencies, particularly for ACh concentrations of 0.001 and 0.01 μM. In the $\mathcal{S}$ model, the combination of Iso and SKb showed strong frequency-dependent effects that decreased with increasing ACh concentration.

Finally, the effects of Iso and SKb on RMP were analyzed and presented in Fig. 6 for a CL of 1000 ms. Corresponding results for CLs of 300 and 500 ms can be found in the Supplementary Material (Fig. 6S). In the $\mathcal{G}$ model, Iso led to a more hyperpolarized RMP, with greater effects observed at shorter cycle lengths, reaching a maximum extra hyperpolarization of 5 mV in control when pacing at a CL of 300 ms. The combination of Iso and SKb produced similar results to those seen with Iso alone, while SKb caused a less negative RMP only for ACh concentrations less than 0.001 μM. The same was true for the $\mathcal{S}$ model, but with weaker effects compared to the $\mathcal{G}$ model. In the $\mathcal{C}$ model, the effects of Iso and SKb on RMP were comparable to those in the $\mathcal{S}$ model, while the combination of Iso and SKb led to a less negative RMP, with the maximum effect observed for a CL of 300 ms.

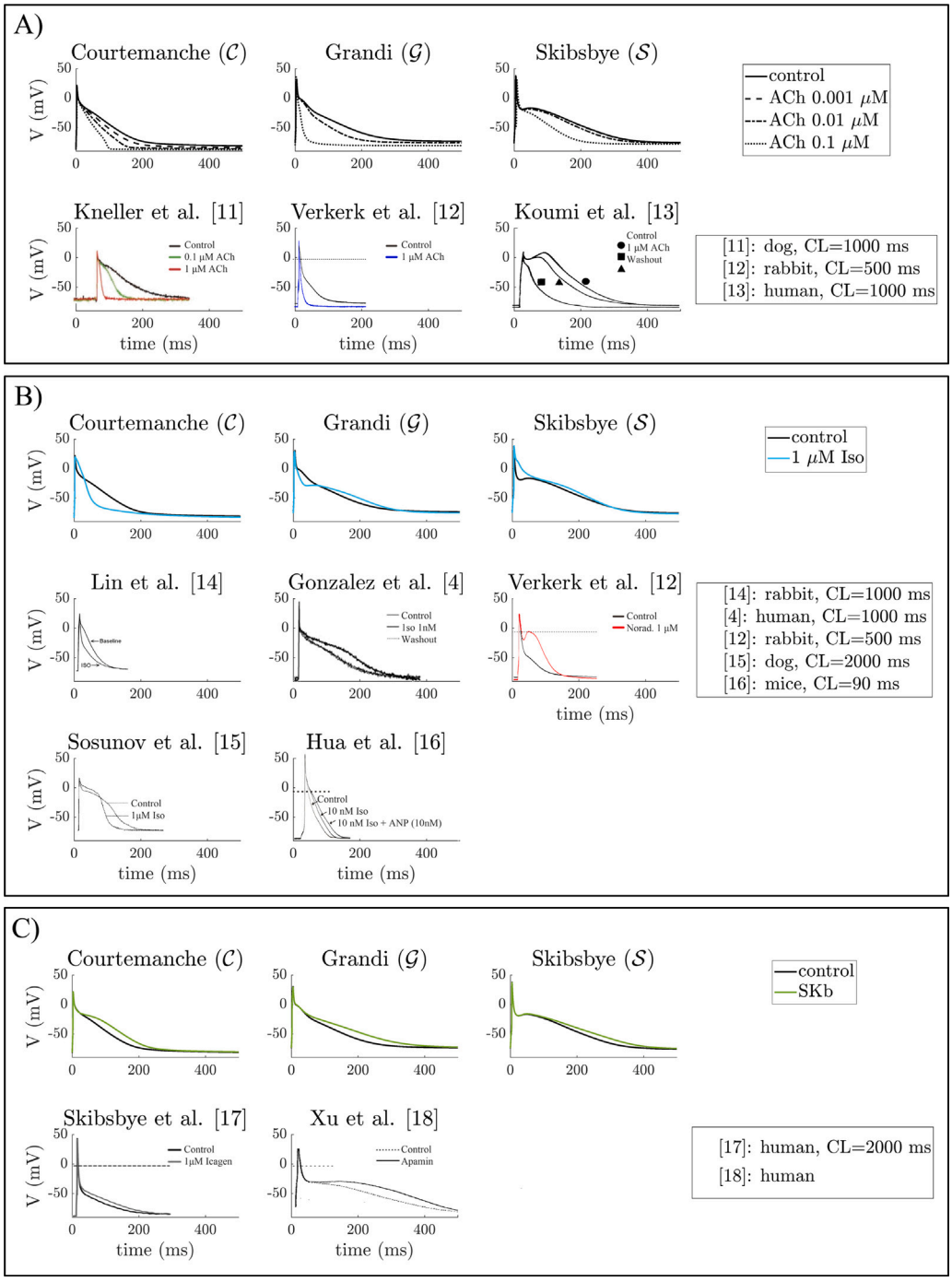

Fig. 4. Comparison of AP traces simulated in this study with experimental AP traces published in the literature. Panel (A) ACh-induced effects. The APs obtained after adding different ACh doses to the $\mathcal{C}$, $\mathcal{G}$ and $\mathcal{S}$ models were compared with experimental results from Koumi et al. [23], Kneller et al. [20] and Verkerk et al. [38]. Panel (B) Iso-induced effects. The APs obtained adding 1 μM Iso to the $\mathcal{C}$, $\mathcal{G}$ and $\mathcal{S}$ models were compared with experimental results from González et al. [13], Hua et al. [39] and Verkerk et al. [38], reporting APD_{90} prolongation, and from Sosunov et al. [12] and Lin et al. [37], reporting APD_{90} shortening. Panel (C) SK block induced effects. The APs obtained after complete SK block in the $\mathcal{C}$, $\mathcal{G}$ and $\mathcal{S}$ models are compared with experimental results from Skibsbye et al. [9] and Xu et al. [40].

3.1.4. *Effects in electrically remodeled cells*

The electrical remodeling caused by psAF resulted in shorter APs compared to non-remodeled myocytes, with APD_{90} being 42.04%, 25.06% and 26.70% shorter in the $\mathcal{C}$, $\mathcal{G}$ and $\mathcal{S}$ models, respectively. The application of ACh further shortened APD_{90} in psAF myocytes by a similar magnitude to that seen in non-remodeled myocytes, as shown in Fig. 7.

SKb had no significant effect on APD_{90} in cholinergically-stimulated myocytes under all tested ACh concentrations and across the three psAF models. This can be attributed to the lower conductance of I_{SK} in psAF cells.

β-adrenergic stimulation by Iso, applied in addition to ACh, prolonged APD_{90} in the $\mathcal{C}$ and $\mathcal{S}$ models of psAF cells to a greater extent than in non-remodeled myocytes. However, in the $\mathcal{G}$ model of psAF

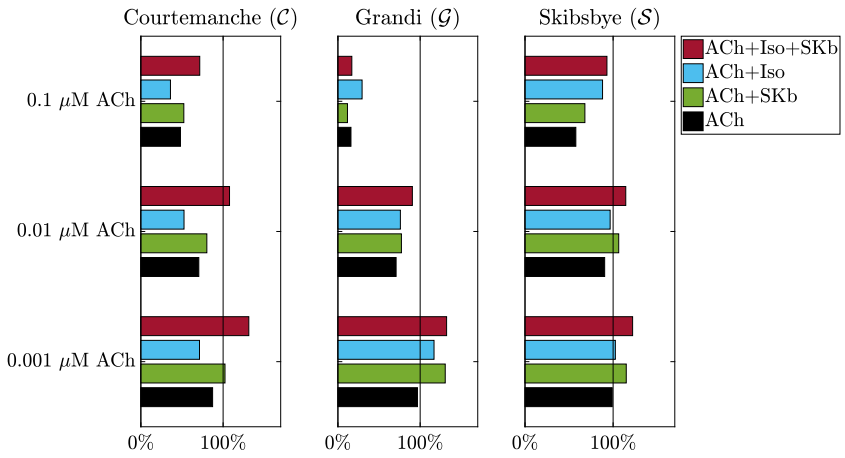

Fig. 5. Percentage of APD_{90} prolongation calculated with respect to the control case (100%) for the different simulated scenarios when pacing at 1000 ms.

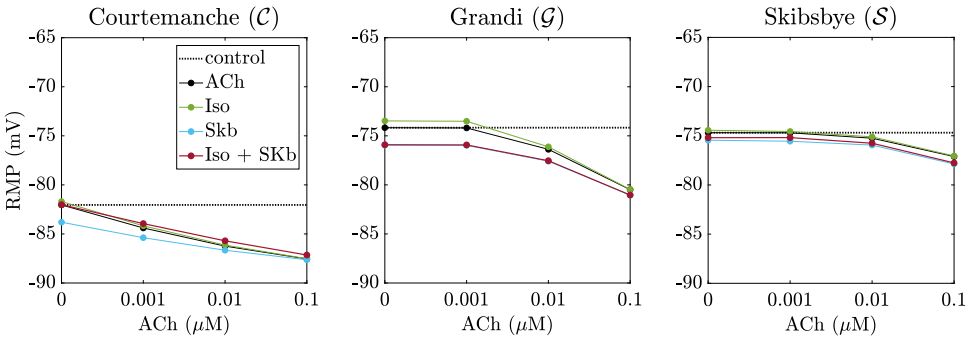

Fig. 6. RMP vs. ACh concentration for human atrial cardiomyocytes models paced at a CL of 1000 ms, at four different tested scenarios comprising cholinergic stimulation individually and in combination with β-adrenergic stimulation and/or SKb.

cells, Iso had no significant effect under all tested ACh concentrations, similar to the results observed in non-remodeled cells.

The combination of Iso and SKb increased the individual effects and resulted in a greater prolongation of APD_{90} in cholinergically-stimulated psAF cells, similar to what was observed in non-remodeled cells. This prolongation brought APD_{90} values near or above baseline for the $\mathcal{C}$ and $\mathcal{S}$ models of psAF cells. However, in the $\mathcal{G}$ model, the APD_{90} prolongation only partially recovered the shortening induced by ACh concentrations of 0.01 and 0.1 μM.

Variations in the RMP in remodeled myocytes were similar to those in non-remodeled myocytes (not displayed).

3.2. Human atrial tissues

3.2.1. Counteraction of ACh-induced changes in activation and repolarization

In non-remodeled tissue, electrical propagation was modestly slowed by 0.1 μM of ACh, resulting in a total activation time increase of 4.5 ms for homogeneous ACh distribution and 2 ms for heterogeneous ACh distribution. The longitudinal CV dropped from 94.56 cm/s at baseline to 86.5 cm/s under homogeneous ACh, which aligns with previous experimental findings [21]. The application of Iso, SKb or a combination of both restored the total activation time to baseline values in both homogeneous and heterogeneous ACh distribution scenarios.

The results of the study indicate that all interventions had a significant impact on APD_{90} in atrial tissues. The homogeneous addition of ACh resulted in a decrease of mean APD_{90} to 87.87 ms and 136.34 ms for 0.1 μM and 0.01 μM ACh respectively, compared to 206.42 ms at baseline. The addition of SKb on top of ACh lengthened mean APD_{90} by 6.13 ms for 0.1 μM ACh and 16.09 ms for 0.01 μM ACh. Conversely, 1 μM Iso had a shortening effect on mean APD_{90} by 23.28 ms and 32.87 ms, respectively. The combination of Iso and SKb counterbalanced the effects of ACh, leading to mean APD_{90} values of 128.96 ms and 206.66 ms for 0.1 μM and 0.01 μM ACh respectively.

For heterogeneous ACh distribution, Fig. 8 shows that the heterogeneous addition of ACh resulted in a decrease in mean APD_{90} by 50.19 ms for 0.1 μM ACh and by 22.59 ms for 0.01 μM ACh. The addition of SKb caused an increase in mean APD_{90} by 22.3 ms and 29.96 ms, respectively. Conversely, 1 μM Iso reduced mean APD_{90} by 31.54 ms and 32.59 ms. The combination of SKb and Iso restored mean APD_{90} to values even greater than at baseline, with values of 224.52 ms and 263.35 ms for 0.1 μM and 0.01 μM ACh, respectively.

3.2.2. Termination of ACh-initiated rotors and prevention of re-induction

β-adrenergic stimulation with 1 μM Iso was able to terminate rotors in cholinergically-stimulated tissues, whether applied alone or in combination with SKb. This was true for all tested application kinetics (Δt_a = 0.1, 1, 5 and 8 s, as shown in Fig. 1) and ACh concentrations (0.01 and 0.1 μM). There was only one exception, which occurred when Iso was applied individually with the highest ACh dose and slowest application kinetics. SKb alone only terminated the rotor under the lowest ACh concentration and with a Δt_a of 8 s. These results are summarized in Fig. 9.

When the application kinetics of Iso and/or SKb was set to Δt_a = 0.1 s, Iso alone and in combination with SKb terminated the rotors in 0.2 s for both ACh concentrations. SKb alone did not terminate the rotor for either ACh concentration. The voltage maps over time for ACh = 0.01 μM are shown in Fig. 7S in the Supplementary Material. The same results were obtained for Δt_a equal to 1, 5, and 8 s, with longer times required to stop the rotors as Δt_a increased.

Two mechanisms were identified to explain rotor termination. After application of Iso or Iso combined with SKb, the rotor extinguished

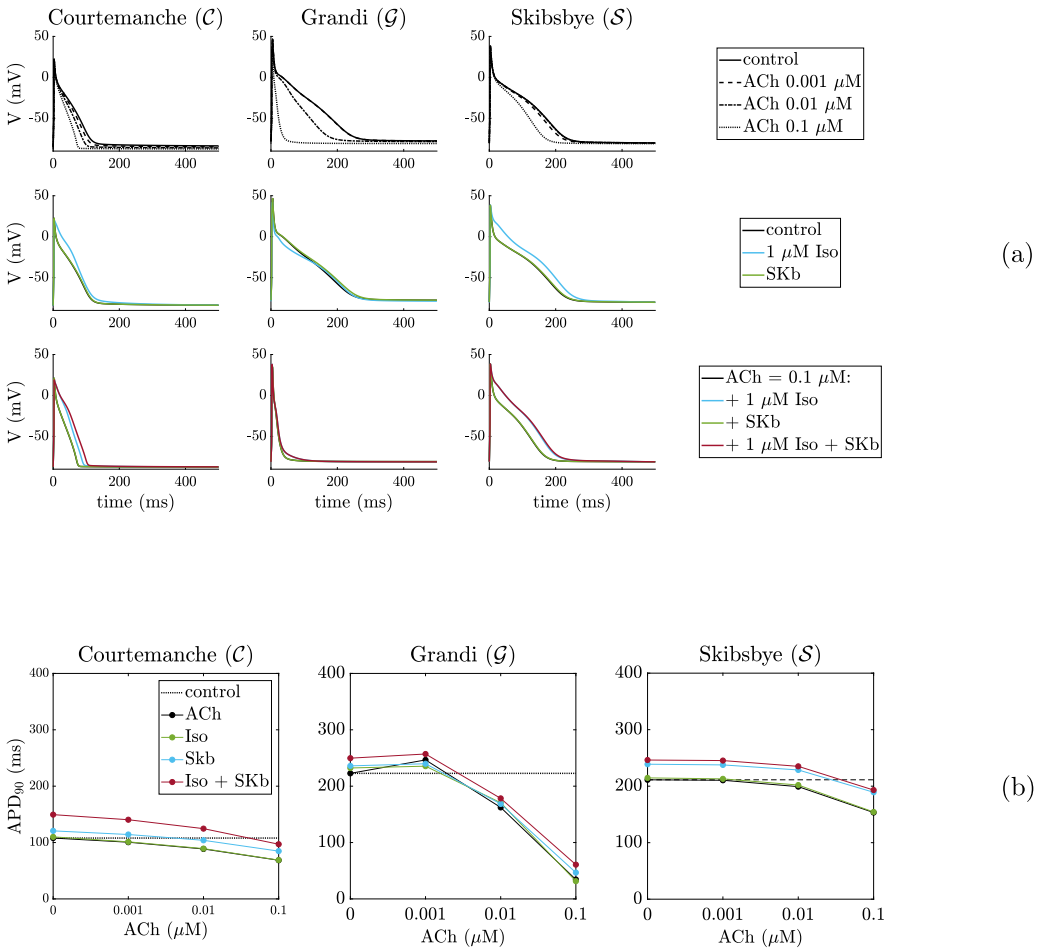

Fig. 7. APs of psAF electrically remodeled human atrial cardiomyocytes paced at a CL of 1000 ms. First row: simulated effects of ACh (concentrations of 0.001, 0.01 and 0.1 μM). Second row: Iso (1 μM concentration) and SKb. Third row: Iso (1 μM concentration) and SKb on top of 0.1 μM ACh (a); APD_{90} vs. ACh concentration for psAF electrically remodeled human atrial myocytes paced at a CL of 1000 ms at four different tested scenarios comprising cholinergic stimulation individually and in combination with β-adrenergic stimulation and/or SKb (b).

due to collision of the rotor tip with the rotor tail, which was likely facilitated by the increased amount of depolarized tissue resulting from prolongation of APD_{90}. In cases where SKb was applied individually, the rotor tip became less stable and started to span larger areas of tissue. In the one case where SKb led to rotor termination, the rotor drifted through the tissue border until it eventually extinguished at the tissue boundaries. To further study these mechanisms, a phase singularity (PS) analysis was performed for Δt_a = 8 s and Δt_a = 5 s using the method described in [41]. Fig. 10 shows two cases: (a) ACh = 0.1 μ M and Δt_a = 8 s, where only Iso combined with SKb was able to stop the rotor, and (b) ACh = 0.01 μ M and Δt_a = 8 s, where the rotor was also stopped by Iso. In all cases, the rotor tip followed a five-pointed star-like trajectory with three long sides and two short sides. The time evolution of this trajectory over 350 ms intervals is shown in Fig. 11. In the first milliseconds after administration of Iso and/or SKb, the rotor tip followed the same trajectory in all studied cases. However, in the Iso and Iso + SKb cases, it soon began to wander and deviate from control. In the SKb cases, deviation from control became apparent later, usually after 8 and 5.5 s from application under 0.1 and 0.01 μ M ACh, respectively.

The results of the PS analysis are presented in the Supplementary Material (Fig. 8S to 15S). This analysis evaluates the movement of rotor tips in terms of the surface covered (A), distance covered (L), and mean velocity ($\overline{V}$), which is defined as the average of the velocities between subsequent PS points. The analysis was conducted over a 10-second period, starting from 2 s after drug application and ending at 12 s. Under control conditions, a lower concentration of 0.01 μM ACh resulted in a larger surface area covered (3.56 cm^2) compared to a higher concentration of 0.1 μM ACh (1.70 cm^2). Adding SKb resulted in an increase in the surface area covered, which was negligible under 0.1 μM ACh, but significant under 0.01 μM ACh. In the latter case, when Δt_a = 5 s, the surface area increased from 3.56 cm^2 to 4.83 cm^2. When Δt_a = 8 s, the surface area increased to 4.95 cm^2. The analysis for the Iso and Iso + SKb cases was more challenging due to early rotor instability. To compare the different therapies, rotor characteristics were analyzed at the same time instant, which was the one preceding instability in the case where it occurred earlier. All cases showed a noticeable increase in the surface area spanned by the rotor tip, with increased rotor meandering potentially due to a larger effective refractory period. The biggest increase in percentage terms was observed for ACh = 0.1 μM and Δt_a = 5 s, where, after 0.85 s from Iso + SKb application, the surface area increased by 109%.

SKb increased the mean velocity under 0.01 μM ACh by 0.79 cm/s and 0.73 cm/s when Δt_a = 5 and 8 s, respectively. Under 0.1 μM ACh, SKb increased the mean velocity by 0.79 cm/s and 0.94 cm/s. Iso and Iso in combination with SKb showed a stronger increase in mean velocity, especially under 0.1 μM ACh. Iso alone increased the mean velocity by 4.39 cm/s and 1.12 cm/s when Δt_a = 5 and 8 s, respectively. When combined with SKb, the mean velocity increased by 3.15 cm/s and 3.52 cm/s.

The re-inducibility of rotors was also tested and the results are summarized in Table 2 for rotors initiated under ACh = 0.01 μM and ACh = 0.1 μM, with Iso or SKb application kinetics defined by Δt_a = 5

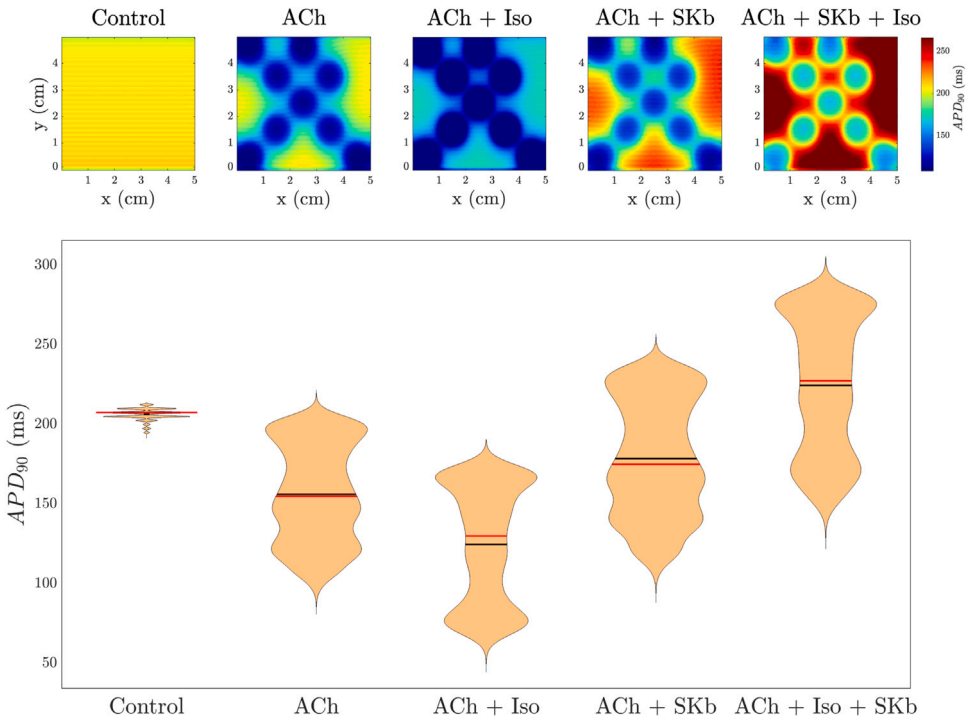

Fig. 8. APD_{90} maps (a) and violin plots (b) at baseline and under 0.1 μM ACh, individually and in combination with 1 μM Iso and/or SKb, for APs defined by the $\mathcal{C}$ model. The APD maps were built from the APD_{90} values computed for the fourth beat at a CL of 1000 ms with the stimulus applied to the bottom edge of the tissue. The violin plots represent the APD_{90} distribution all over the tissue for the different simulated cases. In the violin plots, black lines represent the mean APD_{90} and red lines represent the median APD_{90}.

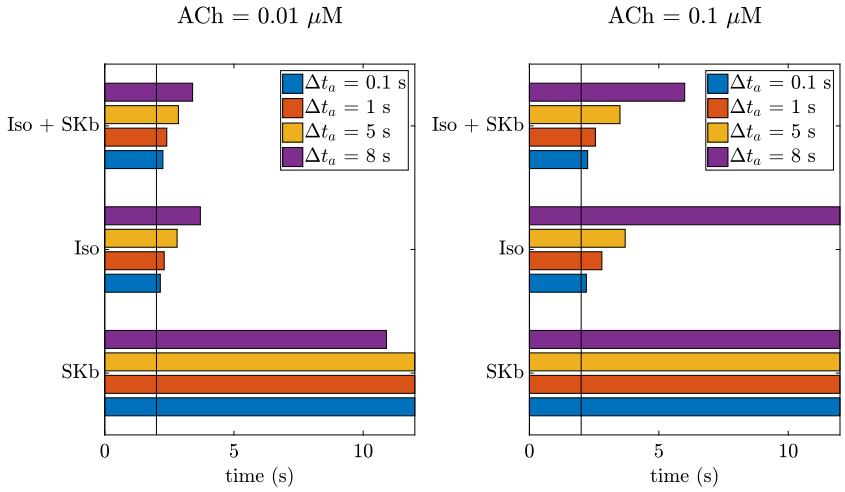

Fig. 9. Time for rotor termination in the different simulated cases. The vertical black line represents the start time of Iso and SKb application. When Iso and SKb act concurrently, the timing is the same for both. Bars arriving to the end of the time scale denote no rotor termination.

s. For Iso and Iso combined with SKb, a narrow range of S1-S2 intervals led to rotor re-initiation, with rotors lasting from 260 ms to 840 ms.

4. Discussion

The impact of inhibiting SK channels and of β-adrenergic stimulation on human atrial myocytes and tissues that have been stimulated by acetylcholine was investigated. To do this, we used existing computational models of atrial cells and added the I_{SK} current and information about the cholinergic and adrenergic modulation of atrial electrical activity, if it was missing. After adding the I_{SK} current to the $\mathcal{C}$ and $\mathcal{G}$ models, we compared the ionic current traces in the original and modified models. The results are presented in Fig. 16S and 17S in the Supplementary Material. In both the $\mathcal{C}$ and $\mathcal{G}$ models, we found that most of the currents were only slightly impacted by the addition of the SK current, with the exception of the rapidly activating delayed rectifier K^+ current (I_{Kr}), which showed a reduction in peak value of 15% and 10% in the $\mathcal{C}$ and $\mathcal{G}$ models, respectively, and of I_{Ks}, which showed a peak reduction of 35% and 31% in the $\mathcal{C}$ and $\mathcal{G}$ models, respectively. Nonetheless, the values of these two currents in the original and modified models were relatively close, especially compared to the wide range of physiological variability reported in experiments, up to 13% for I_{Kr} and 27% for I_{Ks} [42] (Fig. 18S in the Supplementary Material). Based on these results, we concluded that it was not necessary to perform a reparametrization of the cellular models.

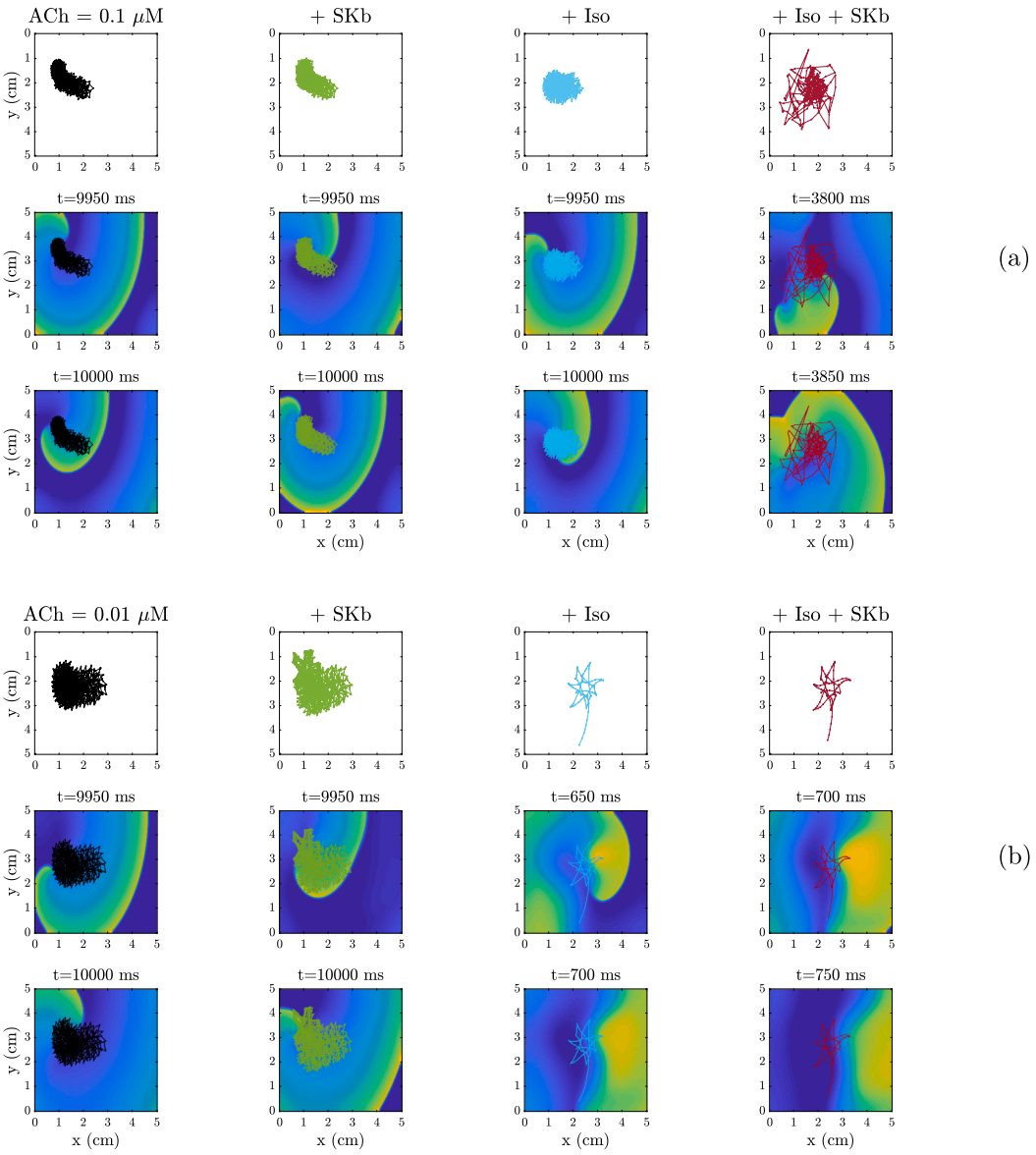

Fig. 10. Phase singularity analysis for 0.1 μM ACh and Δt_a = 8 s (a) and 0.01 μM ACh and Δt_a = 8 s (b). First row: phase singularities in the different tested cases, traced starting from t = 2000 ms. Second and third rows: voltage maps of the rotor at 50 ms before rotor termination or at the end of the simulation if the rotor was not stopped (t = 10000 ms). The color code is the same as in previous figures, with black, green, blue and red representing the effects of ACh, ACh + SKb, ACh + Iso and ACh + Iso + SKb, respectively.

Table 2
Summary of rotor re-inducibility tests, with Δt_a = 5 s. **I-E**: rotor re-initiated but extinguishing.

ACh = 0.01 μM			ACh = 0.1 μM		
S1 (ms)	S1-S2 (ms)	Inducibility	S1 (ms)	S1-S2 (ms)	Inducibility
Iso			Iso		
100	190	**I-E**	100	150	**I-E**
500	190	**I-E**	500	160	**I-E**
1000	180	**I-E**	1000	150	**I-E**
SKb			SKb		
Rotor never stopped. No reinduction			Rotor never stopped. No reinduction		
Iso+SKb			Iso+SKb		
100	200	**I-E**	100	160	**I-E**
500	215	**I-E**	500	200	**I-E**
1000	215	**I-E**	1000	210	**I-E**

In the $\mathcal{C}$, $\mathcal{G}$ and $\mathcal{S}$ models, different formulations were used to model the effects of ACh and Iso. The I_{KACh} formulations were specifically designed for each of the three computational models and were based on different experimental data. These formulations were then introduced in the respective computational models and parametrized to best fit the simulated and experimental data. A similar process was followed in the $\mathcal{G}$ model when the authors introduced their formulations of Iso effects on cellular substrates. In the $\mathcal{C}$ model, the Iso effects were modeled using the formulation by González de la Fuente et al. which was incorporated into the model to reproduce experimental evidence. In the $\mathcal{S}$ model, since no prior Iso models existed, we used the Iso formulation by González de la Fuente et al. [13].

Our models did not take into account the effects of electro-mechanical coupling, but this could be a potential area of future research. In a study by Negroni et al. [16], the authors developed a quantitative framework to examine the interaction between β-adrenergic stimulation and Ca^{2+} transients, AP and contractile properties. As this study only focuses on electrical activity, we do not expect significant differences in our results when simulating the β-adrenergic effects on myofilament properties, as these effects were found to have limited impact on the AP trace and ionic currents. However, this could still be an interesting area for future investigation.

Fig. 11. PS trajectories over time intervals covering 350 ms each, under 0.1 and 0.01 μM ACh applied with kinetics defined by Δt_a of 5 and 8 s. The color code is the same as in the previous figures, with black, green, light blue and red representing individual ACh effect, ACh + SKb, ACh + Iso and ACh + Iso + SKb, respectively.

Regarding our results, we found that SKb, especially in combination with Iso, was able to prolong the APD after ACh had shortened it at both cellular and tissue levels. Iso was also able to reverse arrhythmogenic behaviors induced by ACh, both alone and when combined with SKb. The results presented in this study were calculated using a transverse-to-longitudinal ratio value of 0.5. Different conclusions could be drawn for different anisotropy ratios, as the characteristics of the rotor tip trajectory (area covered, distance traveled, and mean velocity) vary with the ratio. This is demonstrated in Fig. 19S of the Supplementary Material.

We first evaluated the effectiveness of SKb and/or Iso in countering the effects of cholinergic stimulation in single cells. SKb partially countered these effects, with the best results observed for low to moderate cholinergic stimulation corresponding to physiological ACh concentrations up to 0.01 μM. The effects of individual Iso application on the AP were highly dependent on the baseline AP shape, which aligns with previous research findings [43]. The literature contains conflicting results about the effects of Iso on APD. Some studies have reported that Iso leads to shortening of APD [12,37], while others have reported that Iso leads to prolongation of APD [13,38,39]. The literature also contains conflicting results regarding the combination of Iso and ACh, with some studies showing that β-adrenergic stimulation can facilitate AF induction [44] while others have described β-adrenergic stimulation as a brake to reduce the extent of cholinergic-induced APD shortening [12]. These conflicting results could potentially be explained by patient characteristics, with age being identified as a differential factor in animal studies [12].

In our study, Iso-induced APD shortening, which was observed for the $\mathcal{C}$ model, could be attributed to an increase in intracellular calcium concentration due to enhanced release of calcium from the SR. This increased intracellular calcium concentration would activate calcium-activated potassium channels, contributing to APD shortening. Thus, blocking SK channels in addition to Iso was expected to reduce this effect and counteract APD shortening. Indeed, we found that the combination of SK block and Iso was able to reverse ACh effects, prolonging APD to near baseline levels. These results were generally consistent across the three tested models, although the magnitude of Iso and SKb effects was less pronounced for the $\mathcal{G}$ model compared to the $\mathcal{C}$ and $\mathcal{S}$ models.

Next, we tested for frequency-dependent behavior in Iso and SKb, and compared our observations between psAF-remodeled and non-remodeled myocytes. The relative changes in the AP induced by Iso and SKb applied on top of ACh showed minimal frequency dependence, especially for ACh concentrations of 0.01 and 0.1 μM. When comparing the results between psAF-remodeled and non-remodeled cells, we found that the observations were qualitatively similar, with only minor differences in the magnitude of relative changes induced by ACh, Iso and

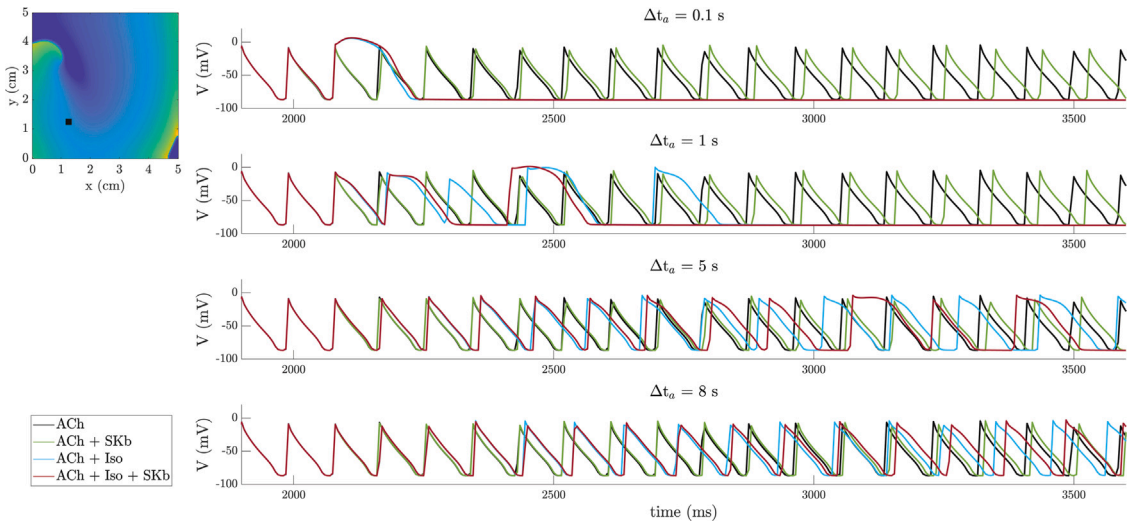

Fig. 12. APs recorded at one point in the tissue (represented with the black square in the top left panel) when applying Iso and/or SKb with kinetics defined by Δt_a of 0.1, 1, 5 and 8 s.

SKb. These changes were of lower amplitude in psAF-remodeled cells than in non-remodeled cells. It is worth mentioning that the effects of SKb were practically negligible in psAF-remodeled cells, which could be due to the lower conductance of SK channels in psAF electrical remodeling.

We then studied the actions of SKb and Iso in tissues with homogeneous and heterogeneous ACh distributions. Our results, in agreement with results at cellular level using the *C* model, showed that individual Iso application further shortened the APD, but the combination of Iso and SKb was able to bring APD back to its baseline value for both homogeneous and heterogeneous ACh distributions and all tested ACh concentrations. For the modeled heterogeneous ACh distribution, spatial APD dispersion was high, but administering Iso combined with SKb remarkably reduced it. We tested the efficacy of various therapies to stop stable rotors in cholinergically-stimulated tissues. The results showed that both Iso and the combination of Iso and SKb were effective in stopping rotors for all tested ACh concentrations and application kinetics, with only one exception for individual Iso. However, individual SKb was only able to stop the rotor in one case, causing it to drift towards the tissue border. The mechanism of rotor termination involved collision between the rotor tail and tip in the cases of individual Iso and combined Iso with SKb. Fig. 12 displays APs recorded in the simulated tissue at a specific point between seconds 2 and 3 for four tested Iso and/or SKb application kinetics. Iso, whether applied individually or in combination with SKb, quickly led to strong prolongation of APD and elevation of AP plateau within the first three seconds of simulation for all tested application kinetics. On the other hand, SK block had slower effects. The transient Iso-induced APD prolongation observed during the first moments after its application is in contrast to the steady-state APD shortening. This transient APD prolongation upon Iso administration is consistent with previous experimental findings [45,46] and has been attributed to differences in the phosphorylation kinetics of I_{Ks} and I_{CaL}, which are two cellular substrates that are altered by sudden, abrupt β-adrenergic stimulation. Both experimental and computational studies have shown that I_{CaL} responds to Iso very quickly, which explains the immediate APD prolongation after Iso administration, while I_{Ks} has a slower response that eventually counteracts the changes in I_{CaL} and leads to APD shortening [45–47]. This kinetic mismatch between I_{CaL} and I_{Ks} has also been observed in response to a gradual increase in Iso concentration [47,48]. Our simulations showed similar observations regarding Iso effects, with even more prominent AP plateau elevation and APD prolongation at the time corresponding to maximum concentration for faster application kinetics (Fig. 12).

The efficacy of Iso and Iso combined with SKb in stopping stable rotors under cholinergic stimulation was further evaluated by examining their ability to prevent re-induction of rotors. Our findings revealed that after the rotor was terminated by Iso alone or in combination with SKb, it could not be re-initiated within the next minute. When re-induced later, the rotor persisted for a maximum of 840 ms.

Based on these results, we can conclude that the combination of Iso and SKb may serve as an effective therapy to mitigate the harmful effects of ACh in the human atria. This conclusion is supported by the ability of combined Iso and SKb to prolong APD at steady state and to aid in cardioversion and maintenance of the restored sinus rhythm.

5. Study limitations

The study had some limitations that should be considered for future research. Our investigation aimed to evaluate the effectiveness of Iso and SKb in counteracting the cholinergic effects on human atrial cells and tissues. The simulations were performed at the cellular level and on 2D tissue sheets, but did not include the regional electrophysiological heterogeneities and cell-to-cell variability that exist in real human atria. This study highlights the importance of biological variability in drug evaluation and future research could include populations of cell models to account for this variability [49]. Another avenue for future investigation would be to use 3D whole-atrial models to better understand complex rotor behavior and rotor termination mechanisms.

The results of this study emphasize the non-steady-state kinetics of Iso as a factor in its impact on rotor termination. Further research using biophysically-detailed β-adrenergic signaling models could examine the effects of different Iso concentrations and help to understand its potential as an anti-arrhythmic therapy, particularly when combined with SK channel inhibition delivered with possibly different administration kinetics as those for Iso.

It is important to note that cellular models have limitations due to the scarce experimental human data and the large variability displayed by human atrial cells and tissues. Additionally, the Courtemanche model has a limitation in its simplified modeling of SR Ca^{2+} handling due to limited data on Ca^{2+} storage and release kinetics from the SR at the time the model was developed.

6. Conclusion

First, the impact of Iso and SKb on human atrial cardiomyocytes was evaluated. The ability of individual SKb to restore the APD shortening

induced by ACh was observed, with the change ranging from 5% to 170% depending on the ACh concentration. The effects of SKb were, however, reduced in electrically remodeled cells. Additionally, when SKb was used to stop sustained rotors initiated under cholinergic stimulation, its effects were insufficient. On the other hand, Iso was successful in terminating rotors, but its impact on APD varied depending on the baseline AP morphology. The combination of Iso and SKb resulted in stronger APD prolongation at steady state, which effectively countered the shortening induced by ACh, restoring from 67% to 250% of the APD shortening. The combination of Iso and SKb was also successful in stopping stable rotors and preventing their reinducibility. Previous studies have explored the interactions between parasympathetic and sympathetic actions, as well as between parasympathetic activity and SKb, but this study is the first to consider the complex interactions between ACh, Iso and SKb. The results support the possibility of using a combination of SK channel block and β-adrenergic stimulation as a therapy to counteract the potential arrhythmogenic effects of cholinergic stimulation in human atria.

CRediT authorship contribution statement

Chiara Celotto: Designed the study, Analyzed the results, Drafted the manuscript, Performed the electrophysiological simulations, Developed the post-processing software and performed the required computation. **Carlos Sánchez:** Designed the study, Analyzed the results, Supervised and formalized the project and were responsible for overseeing the research and providing criticalinsight and recommendations regarding the focus, structure and content of the paper. **Konstantinos A. Mountris:** Contributed with technical details. **Pablo Laguna:** Designed the study, Analyzed the results, Supervised and formalized the project and were responsible for overseeing the research and providing criticalinsight and recommendations regarding the focus, structure and content of the paper. **Esther Pueyo:** Designed the study, Analyzed the results, Supervised and formalized the project and were responsible for overseeing the research and providing criticalinsight and recommendations regarding the focus, structure and content of the paper.

Declaration of competing interest

The authors declare that they have no known competing financial interests or personal relationships that could have appeared to influence the work reported in this paper.

Acknowledgments

This work was supported by projects PID2019-105674RB-I00, PID2019-104881RB-I00 and TED2021-130459B-I00(Ministerio de Ciencia e Innovación and European Social Fund), Spain, ERC G.A., Spain 638284 (ERC), Marie Skłodowska-Curie ITN, Spain grant 766082 MYATRIA (European Commission) and by European Social Fund (EU) and Aragón Government, Spain through project LMP94_21 and BSICoS group, Spain T39_23R. Computations were performed by the ICTS NANBIOSIS (HPC Unit at University of Zaragoza).

Appendix A. Supplementary data

Supplementary material related to this article can be found online at https://doi.org/10.1016/j.compbiomed.2023.106719.

References

[1] Massimo Zoni-Berisso, Fabrizio Lercari, Tiziana Carazza, Stefano Domenicucci, Epidemiology of atrial fibrillation: European perspective, Clin. Epidemiol. 6 (2014) 213–220.
[2] Hans Kottkamp, Doreen Schreiber, Fabian Moser, Andreas Rieger, Therapeutic approaches to atrial fibrillation ablation targeting atrial fibrosis, JACC. Clin. Electrophysiol. 3 (7) (2017) 643–653.
[3] Jay Chen, Stephen L. Wasmund, Mohamed H. Hamdan, Back to the future: The role of the autonomic nervous system in atrial fibrillation, Pacing Clin. Electrophysiol. 29 (4) (2006) 413–421.
[4] Peng-Sheng Chen, Lan S. Chen, Michael C. Fishbein, Shien-Fong Lin, Stanley Nattel, Role of the autonomic nervous system in atrial fibrillation, Circ. Res. 114 (9) (2014) 1500–1515.
[5] Ching-Tai Tai, Role of autonomic influences in the initiation and perpetuation of focal atrial fibrillation, J. Cardiovasc. Electrophysiol. 12 (3) (2001) 292–293.
[6] P. Coumel, Paroxysmal atrial fibrillation: a disorder of autonomic tone? Eur. Heart J. 15 Suppl A (1994) 9–16.
[7] Kazuki Iso, Yasuo Okumura, Ichiro Watanabe, Koichi Nagashima, Keiko Takahashi, Masaru Arai, Ryuta Watanabe, Yuji Wakamatsu, Naoto Otsuka, Seina Yagyu, Sayaka Kurokawa, Toshiko Nakai, Kimie Ohkubo, Atsushi Hirayama, Is vagal response during left atrial ganglionated plexi stimulation a normal phenomenon? Circulation 12 (10) (2019) e007281.
[8] Ravi Mandapati, Allan Skanes, Jay Chen, Omer Berenfeld, José Jalife, Stable microreentrant sources as a mechanism of atrial fibrillation in the isolated sheep heart, Circulation 101 (2) (2000) 194–199.
[9] Lasse Skibsbye, Claire Poulet, Jonas Goldin Diness, Bo Hjorth Bentzen, Lei Yuan, Utz Kappert, Klaus Matschke, Erich Wettwer, Ursula Ravens, Morten Grunnet, Torsten Christ, Thomas Jespersen, Small-conductance calcium-activated potassium (SK) channels contribute to action potential repolarization in human atria, Cardiovasc. Res. 103 (1) (2014) 156–167.
[10] Stanley Nattel, Calcium-activated potassium current: a novel ion channel candidate in atrial fibrillation, J. Physiol. 587 (7) (2009) 1385–1386.
[11] Lasse Skibsbye, Jonas Goldin Diness, Ulrik Svane Sørensen, Rie Schultz Hansen, Morten Grunnet, The duration of pacing-induced atrial fibrillation is reduced in vivo by inhibition of small conductance Ca(2+)-activated K(+) channels, J. Cardiovasc. Pharmacol. 57 (6) (2011) 672–681.
[12] Eugene A. Sosunov, Evgeny P. Anyukhovsky, Michael R. Rosen, Adrenergic-cholinergic interaction that modulates repolarization in the atrium is altered with aging, J. Cardiovasc. Electrophysiol. 13 (4) (2002) 374–379.
[13] Marta González de la Fuente, Adriana Barana, Ricardo Gómez, Irene Amorós, Pablo Dolz-Gaitón, Sandra Sacristán, Felipe Atienza, Ana Pita, Ángel Pinto, Francisco Fernández-Avilés, Ricardo Caballero, Juan Tamargo, Eva Delpón, Chronic atrial fibrillation up-regulates β 1-adrenoceptors affecting repolarizing currents and action potential duration, Cardiovasc. Res. 97 (2) (2013) 379–388.
[14] S.L. Stuesse, D.W. Wallick, M.N. Levy, Autonomic control of right atrial contractile strength in the dog, Am. J. Physiol. 236 (6) (1979) H860–865.
[15] K.B. Walsh, T.B. Begenisich, R.S. Kass, Beta-adrenergic modulation in the heart. independent regulation of K and Ca channels, Pflugers Arch.: Eur. J. Physiol. 411 (2) (1988) 232–234.
[16] Jorge A. Negroni, Stefano Morotti, Elena C. Lascano, Aldrin V. Gomes, Eleonora Grandi, José L. Puglisi, Donald M. Bers, β -Adrenergic effects on cardiac myofilaments and contraction in an integrated rabbit ventricular myocyte model, J. Mol. Cell. Cardiol. 81 (2015) 162–175.
[17] Mathias Wilhelms, Hanne Hettmann, Mary M. Maleckar, Jussi T. Koivumäki, Olaf Dössel, Gunnar Seemann, Benchmarking electrophysiological models of human atrial myocytes, Front. Physiol. 3 (2012) 487.
[18] Marc Courtemanche, Rafael J. Ramirez, Stanley Nattel, Ionic mechanisms underlying human atrial action potential properties: Insights from a mathematical model, Am. J. Physiol.-Heart Circ. Physiol. 275 (1) (1998) H301–H321.
[19] Eleonora Grandi, Sandeep V. Pandit, Niels Voigt, Antony J. Workman, Dobromir Dobrev, José Jalife, Donald M. Bers, Human atrial action potential and Ca2+ model: Sinus rhythm and chronic atrial fibrillation, Circ. Res. 109 (9) (2011) 1055–1066.
[20] James Kneller, Renqiang Zou, Edward J. Vigmond, Zhiguo Wang, L. Joshua Leon, Stanley Nattel, Cholinergic atrial fibrillation in a computer model of a two-dimensional sheet of canine atrial cells with realistic ionic properties, Circ. Res. 90 (9) (2002).
[21] Jason D. Bayer, Bastiaan J. Boukens, Sébastien P.J. Krul, Caroline H. Roney, Antoine H.G. Driessen, Wouter R. Berger, Nicoline W.E. van den Berg, Arie O. Verkerk, Edward J. Vigmond, Ruben Coronel, Joris R. de Groot, Acetylcholine delays atrial activation to facilitate atrial fibrillation, Front. Physiol. 10 (2019) 1105.
[22] Niels Voigt, Jordi Heijman, Anne Trausch, Elisa Mintert-Jancke, Lutz Pott, Ursula Ravens, Dobromir Dobrev, Impaired Na+-dependent regulation of acetylcholine-activated inward-rectifier K+ current modulates action potential rate dependence in patients with chronic atrial fibrillation, J. Mol. Cell. Cardiol. 61 (2013) 142–152.

[23] S. Koumi, C.E. Arentzen, C.L. Backer, J.A. Wasserstrom, Alterations in muscarinic K+ channel response to acetylcholine and to g protein-mediated activation in atrial myocytes isolated from failing human hearts, Circulation 90 (5) (1994) 2213–2224.

[24] Thomas R. Shannon, Fei Wang, Donald M. Bers, Regulation of cardiac sarcoplasmic reticulum Ca release by luminal [Ca] and altered gating assessed with a mathematical model, Biophys. J. 89 (6) (2005) 4096–4110.

[25] Lasse Skibsbye, Thomas Jespersen, Torsten Christ, Mary M. Maleckar, Jonas van den Brink, Pasi Tavi, Jussi T. Koivumäki, Refractoriness in human atria: Time and voltage dependence of sodium channel availability, J. Mol. Cell. Cardiol. 101 (2016) 26–34.

[26] Jutta Engel, Howard A. Schultens, Detlev Schild, Small conductance potassium channels cause an activity-dependent spike frequency adaptation and make the transfer function of neurons logarithmic, Biophys. J. 76 (3) (1999) 1310–1319.

[27] Angelina Peñaranda, Blas Echebarria, Enrique Alvarez-Lacalle, Inmaculada R. Cantalapiedra, Effects of small conductance calcium activated potassium channels in cardiac myocytes, Comput. Cardiol. 44 (2017) 1–4.

[28] Chia-Hsiang Hsueh, Po-Cheng Chang, Yu-Cheng Hsieh, Thomas Reher, Peng-Sheng Chen, Shien-Fong Lin, Proarrhythmic effect of blocking the small conductance calcium activated potassium channel in isolated canine left atrium, Heart Rhythm. 10 (6) (2013) 891–898.

[29] Chiara Celotto, Carlos Sánchez, Pablo Laguna, Esther Pueyo, Calcium-activated potassium channel inhibition in autonomically stimulated human atrial myocytes, Comput. Cardiol. 46 (2019) 1–4.

[30] M. Courtemanche, Ionic targets for drug therapy and atrial fibrillation-induced electrical remodeling: Insights from a mathematical model, Cardiovasc. Res. 42 (2) (1999) 477–489.

[31] Samuel Sossalla, Birte Kallmeyer, Stefan Wagner, Marek Mazur, Ulrike Maurer, Karl Toischer, Jan D. Schmitto, Ralf Seipelt, Friedrich A. Schöndube, Gerd Hasenfuss, Luiz Belardinelli, Lars S. Maier, Altered na(+) currents in atrial fibrillation effects of ranolazine on arrhythmias and contractility in human atrial myocardium number = 21, J. Am. Coll. Cardiol. 55 (21) (2010) 2330–2342.

[32] N. Voigt, A.W. Trafford, U. Ravens, D. Dobrev, Cellular and molecular determinants of altered atrial Ca2+ signaling in patients with chronic atrial fibrillation, Circulation.

[33] Konstantinos A. Mountris, Esther Pueyo, The radial point interpolation mixed collocation method for the solution of transient diffusion problems, Eng. Anal. Bound. Elem. 121 (2020) 207–216.

[34] Konstantinos A. Mountris, Esther Pueyo, Next-generation in silico cardiac electrophysiology through immersed grid meshfree modeling: application to simulation of myocardial infarction, Comput. Cardiol. 47 (2020) 1–4.

[35] Konstantinos A. Mountris, Leiting Dong, Yue Guan, Satya N. Atluri, Esther Pueyo, Meshfree implementation of the cardiac monodomain model through the fragile points method, Methods 11 (2021) 12.

[36] Elhacene Matene, Alain Vinet, Vincent Jacquemet, Dynamics of atrial arrhythmias modulated by time-dependent acetylcholine concentration: a simulation study, Europace 16 Suppl 4 (2014) iv11–iv20.

[37] Yung-Kuo Lin, Yao-Chang Chen, Jen-Hung Huang, Yenn-Jiang Lin, Shiang-Suo Huang, Shih-Ann Chen, Yi-Jen Chen, Leptin modulates electrophysiological characteristics and isoproterenol-induced arrhythmogenesis in atrial myocytes, J. Biomed. Sci. 20 (1) (2013) 94.

[38] Arie O. Verkerk, Guillaume S.C. Geuzebroek, Marieke W. Veldkamp, Ronald Wilders, Effects of acetylcholine and noradrenalin on action potentials of isolated rabbit sinoatrial and atrial myocytes, Front. Physiol. 3 (2012).

[39] Rui Hua, Sarah L. MacLeod, Iuliia Polina, Motahareh Moghtadaei, Hailey J. Jansen, Oleg Bogachev, Stacy B. O'Blenes, John L. Sapp, Jean-Francois Legare, Robert A. Rose, Effects of wild-type and mutant forms of atrial natriuretic peptide on atrial electrophysiology and arrhythmogenesis, Circ. Arrhythm. Electrophysiol. 8 (5) (2015) 1240–1254.

[40] Yanfang Xu, Dipika Tuteja, Zhao Zhang, Danyan Xu, Yi Zhang, Jennifer Rodriguez, Liping Nie, Holly R. Tuxson, J. Nilas Young, Kathryn A. Glatter, Ana E. Vázquez, Ebenezer N. Yamoah, Nipavan Chiamvimonvat, Molecular identification and functional roles of a Ca(2+)-activated K+ channel in human and mouse hearts, J. Biol. Chem. 278 (49) (2003) 49085–49094.

[41] Philippe Comtois, Masao Sakabe, Edward J. Vigmond, Mauricio Munoz, Anne Texier, Akiko Shiroshita-Takeshita, Stanley Nattel, Mechanisms of atrial fibrillation termination by rapidly unbinding na+ channel blockers: Insights from mathematical models and experimental correlates, Am. J. Physiol. Heart Circ. Physiol. 295 (4) (2008) H1489–1504.

[42] Zsófia Kohajda, László Virág, Tibor Hornyik, Zoltán Husti, Anita Sztojkov-Ivanov, Norbert Nagy, András Horváth, Richárd Varga, János Prorok, Jozefina Szlovák, Noémi Tóth, Péter Gazdag, Leila Topal, Muhammad Naveed, Tamás Árpádffy-Lovas, Bence Pászti, Tibor Magyar, István Koncz, Szilvia Déri, Vivien Demeter-Haludka, Zoltán Aigner, Balázs Ördög, Márta Patfalusi, László Tálosi, László Tiszlavicz, Imre Földesi, Norbert Jost, István Baczkó, András Varró, In vivo and cellular antiarrhythmic and cardiac electrophysiological effects of desethylamiodarone in dog cardiac preparations, Br. J. Pharmacol. 179 (13) (2022) 3382–3402.

[43] N. Szentandrássy, V. Farkas, L. Bárándi, B. Hegyi, F. Ruzsnavszky, B. Horváth, T. Bányász, J. Magyar, I. Márton, P.P. Nánási, Role of action potential configuration and the contribution of C^2+ and K+ currents to isoprenaline-induced changes in canine ventricular cells, Br. J. Pharmacol. 167 (3) (2012) 599–611.

[44] Rishi Arora, Recent insights into the role of the autonomic nervous system in the creation of substrate for atrial fibrillation: Implications for therapies targeting the atrial autonomic nervous system, Circ. Arrhythm. Electrophysiol. 5 (4) (2012) 850–859.

[45] Gong-Xin Liu, Bum-Rak Choi, Ohad Ziv, Weiyan Li, Enno de Lange, Zhilin Qu, Gideon Koren, Differential conditions for early after-depolarizations and triggered activity in cardiomyocytes derived from transgenic LQT1 and LQT2 rabbits, J. Physiol. 590 (5) (2012) 1171–1180.

[46] Yuanfang Xie, Eleonora Grandi, Jose L. Puglisi, Daisuke Sato, Donald M. Bers, β -Adrenergic stimulation activates early afterdepolarizations transiently via kinetic mismatch of PKA targets, J. Mol. Cell. Cardiol. 58 (2013) 153–161.

[47] David Adolfo Sampedro-Puente, Jesus Fernandez-Bes, Norbert Szentandrássy, Péter Nánási, Peter Taggart, Esther Pueyo, Time course of low-frequency oscillatory behavior in human ventricular repolarization following enhanced sympathetic activity and relation to arrhythmogenesis, Front. Physiol. 10 (2019) 1547.

[48] Esther Pueyo, Michele Orini, José F. Rodríguez, Peter Taggart, Interactive effect of beta-adrenergic stimulation and mechanical stretch on low-frequency oscillations of ventricular action potential duration in humans, J. Mol. Cell. Cardiol. 97 (2016) 93–105.

[49] Elisa Passini, Xin Zhou, Cristian Trovato, Oliver J Britton, Alfonso Bueno-Orovio, Blanca Rodriguez, The virtual assay software for human in silico drug trials to augment drug cardiac testing, J. Comput. Sci. 52 (2021) 101202.

Supplementary Material

Chiara Celotto[a,b,1], Carlos Sánchez[a,b], Konstantinos A. Mountris[c], Pablo Laguna[a,b], Esther Pueyo[a,b]

[a] *BSICoS Group, I3A and IIS-Aragón, University of Zaragoza, Spain*
[b] *CIBER - Bioingeniería, Biomateriales, y Nanomedicina (CIBER-BBN), Zaragoza, Spain*
[c] *UCL Mechanical Engineering, London, UK*

References

[1] A. O. Verkerk, G. S. C. Geuzebroek, M. W. Veldkamp, R. Wilders, Effects of Acetylcholine and Noradrenalin on Action Potentials of Isolated Rabbit Sinoatrial and Atrial Myocytes, Frontiers in Physiology 3. doi:10.3389/fphys.2012.00174.

[2] C.-H. Hsueh, P.-C. Chang, Y.-C. Hsieh, T. Reher, P.-S. Chen, S.-F. Lin, Proarrhythmic Effect of Blocking the Small Conductance Calcium Activated Potassium Channel in Isolated Canine Left Atrium, Heart Rhythm 10 (6) (2013) 891–898. doi:10.1016/j.hrthm.2013.01.033.

[3] L. Skibsbye, C. Poulet, J. G. Diness, B. H. Bentzen, L. Yuan, U. Kappert, K. Matschke, E. Wettwer, U. Ravens, M. Grunnet, T. Christ, T. Jespersen, Small-Conductance Calcium-Activated Potassium (SK) Channels Contribute to Action Potential Repolarization in Human Atria, Cardiovascular Research 103 (1) (2014) 156–167. doi:10.1093/cvr/cvu121.

[4] Z. Kohajda, L. Virág, T. Hornyik, Z. Husti, A. Sztojkov-Ivanov, N. Nagy, A. Horváth, R. Varga, J. Prorok, J. Szlovák, N. Tóth, P. Gazdag, L. Topal, M. Naveed, T. Árpádffy Lovas, B. Pászti, T. Magyar, I. Koncz, S. Déri, V. Demeter-Haludka, Z. Aigner, B. Ördög, M. Patfalusi, L. Tálosi, L. Tiszlavicz, I. Földesi, N. Jost, I. Baczkó, A. Varró, In Vivo and Cellular Antiarrhythmic and Cardiac Electrophysiological Effects of Desethylamiodarone in Dog Cardiac Preparations, British Journal of Pharmacology 179 (13) (2022) 3382–3402. doi:10.1111/bph.15812.

[1] Chiara Celotto, email: chiaracelotto@unizar.es, telephone number: +393473144689

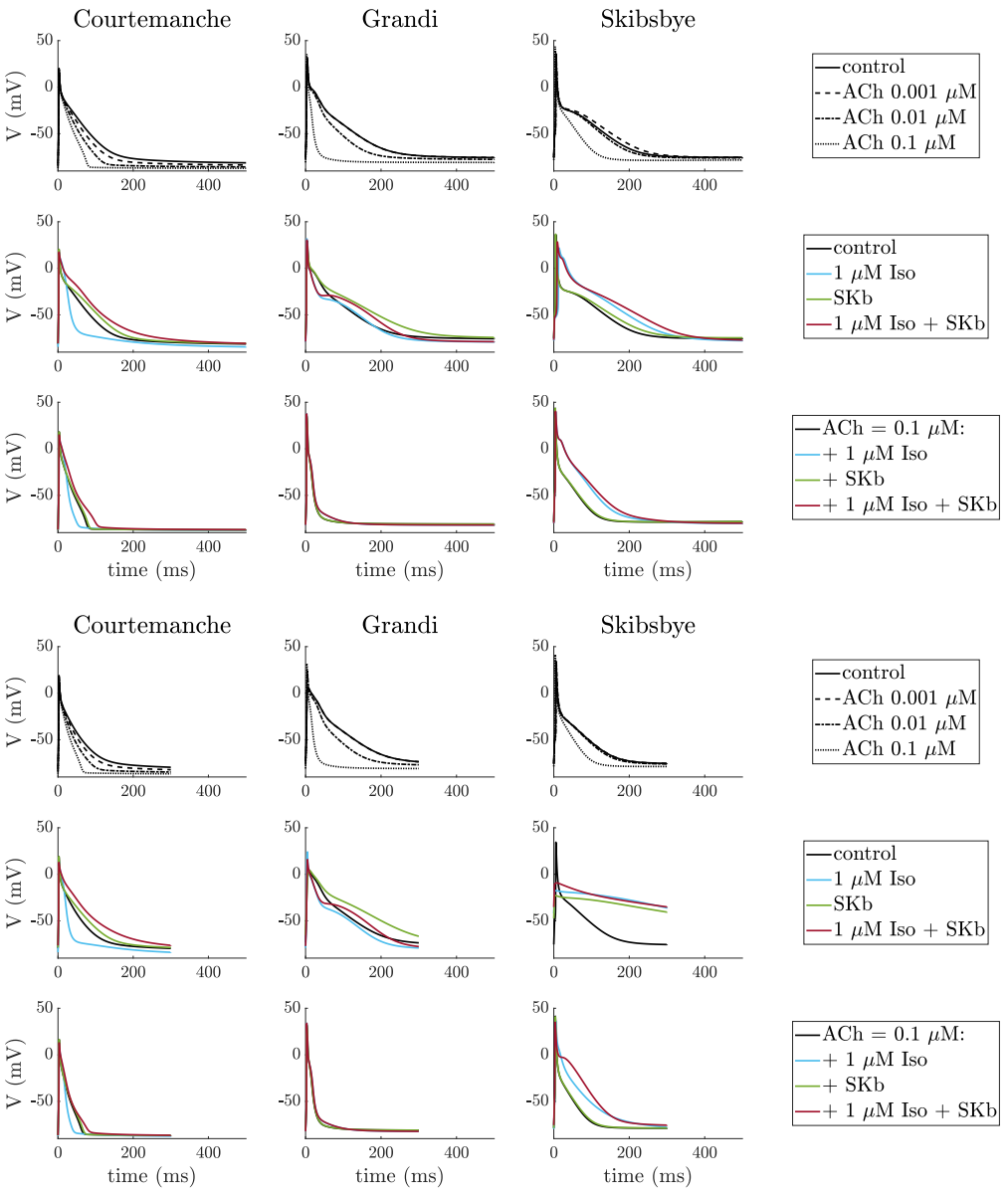

Figure 1S: APs of human atrial cardiomyocytes models paced at a CL of 500 ms (a) and of 300 ms (b). First row: simulated effects of ACh (at concentrations of 0.001, 0.01 and 0.1 μM). Second row: Iso (at a 1 μM concentration) and SKb. Third row: Iso (at a 1 μM concentration) and SKb on top of 0.1 μM ACh. When pacing the $\mathcal{S}$ model at a CL of 300 ms, the AP was not able to fully repolarize under ACh combined with Iso and/or SKb.

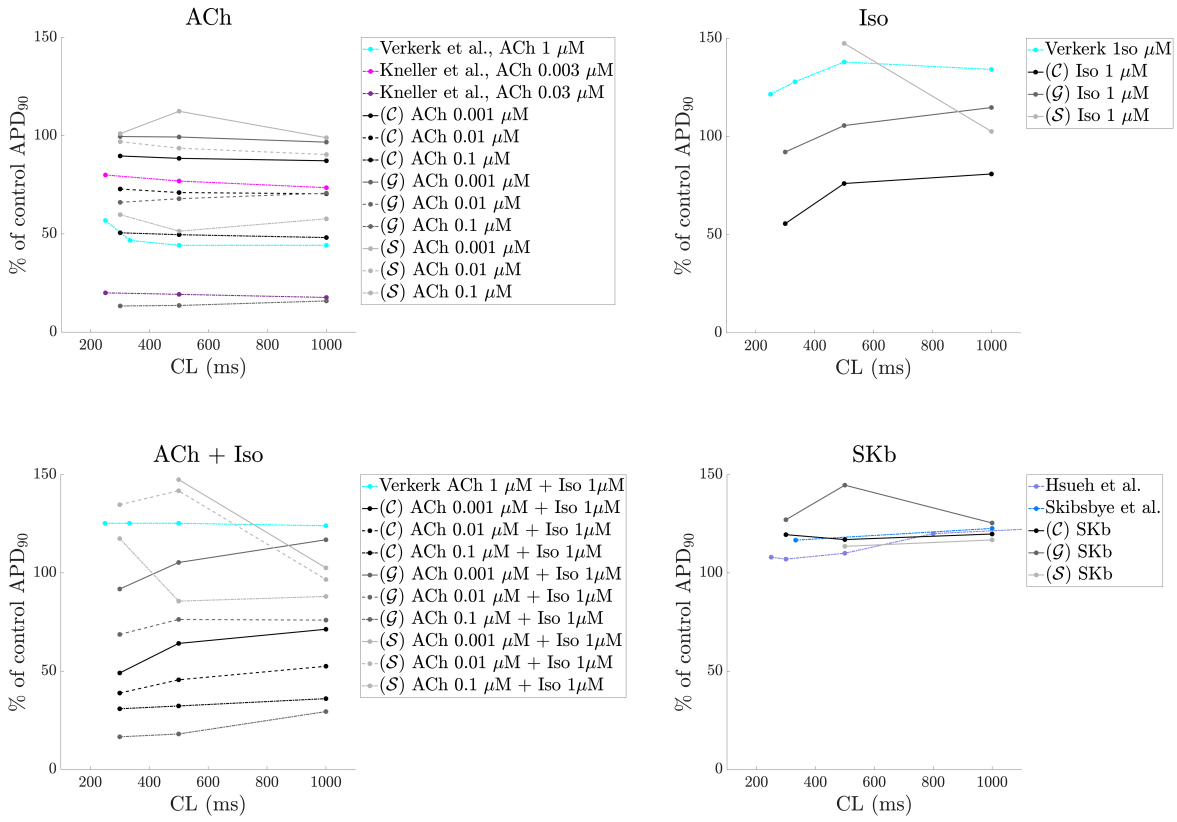

Figure 2S: Percentages of change in APD_{90} with respect to the APD_{90} value in control when pacing at different CLs. Simulation results were compared with data published in the literature. Panel A) ACh-induced effects. The APD_{90} obtained after adding different ACh doses in the $\mathcal{C}$, $\mathcal{G}$ and $\mathcal{S}$ models at different pacing CLs were compared with experimental results from Verkerk et al. [1]. Panel B) Iso-induced effects. Simulation results were compared with experimental results by Verkerk et al. [1]. Panel C) ACh + Iso-induced effects. Simulation results were compared with experimental results by Verkerk et al. Panel D) SKb-induced effects. Simulation results were compared with experimental results by Hsueh et al. [2] and by Skibsbye et al. [3]

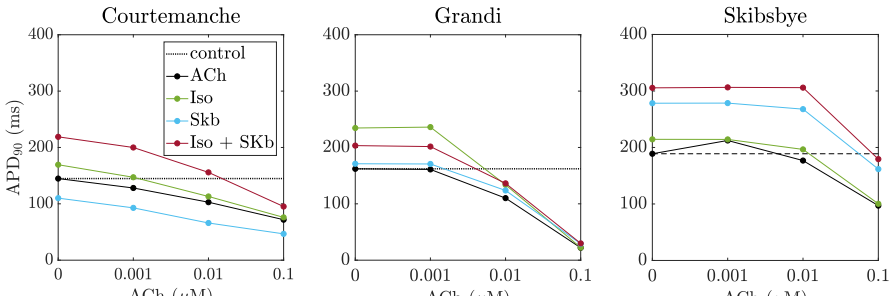

(a)

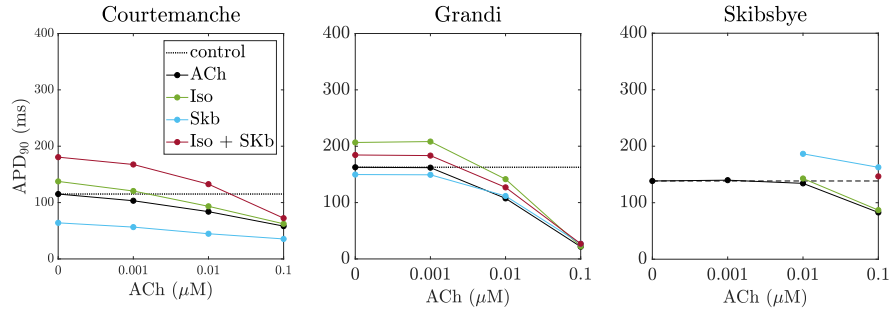

(b)

Figure 3S: APD_{90} vs ACh concentration for human atrial myocytes models paced a CL of 500 ms (a) and 300 ms (b) at four different tested scenarios comprising cholinergic stimulation individually and in combination with β-adrenergic stimulation and/or SKb.

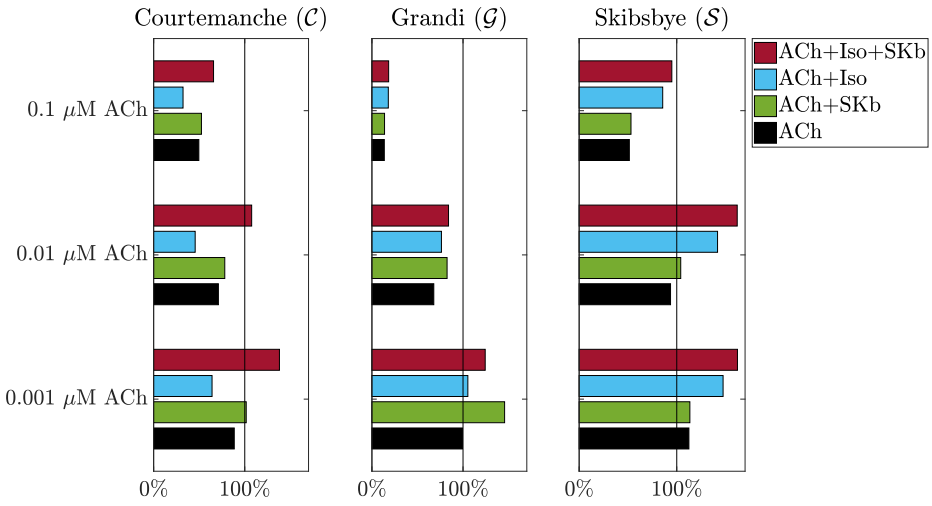

Figure 4S: Percentage of APD_{90} prolongation calculated with respect to the control case (100%) for the different simulated scenarios when pacing at 500 ms.

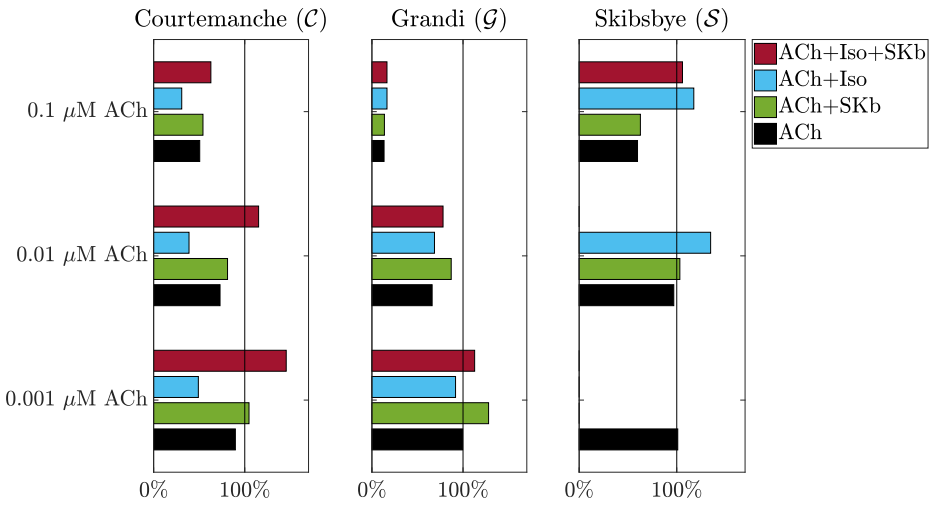

Figure 5S: Percentage of APD_{90} prolongation calculated with respect to the control case (100%) for the different simulated scenarios when pacing at 300 ms. The AP was not able to fully repolarize under ACh combined with Iso and/or SKb and the corresponding bars are not represented in the figure.

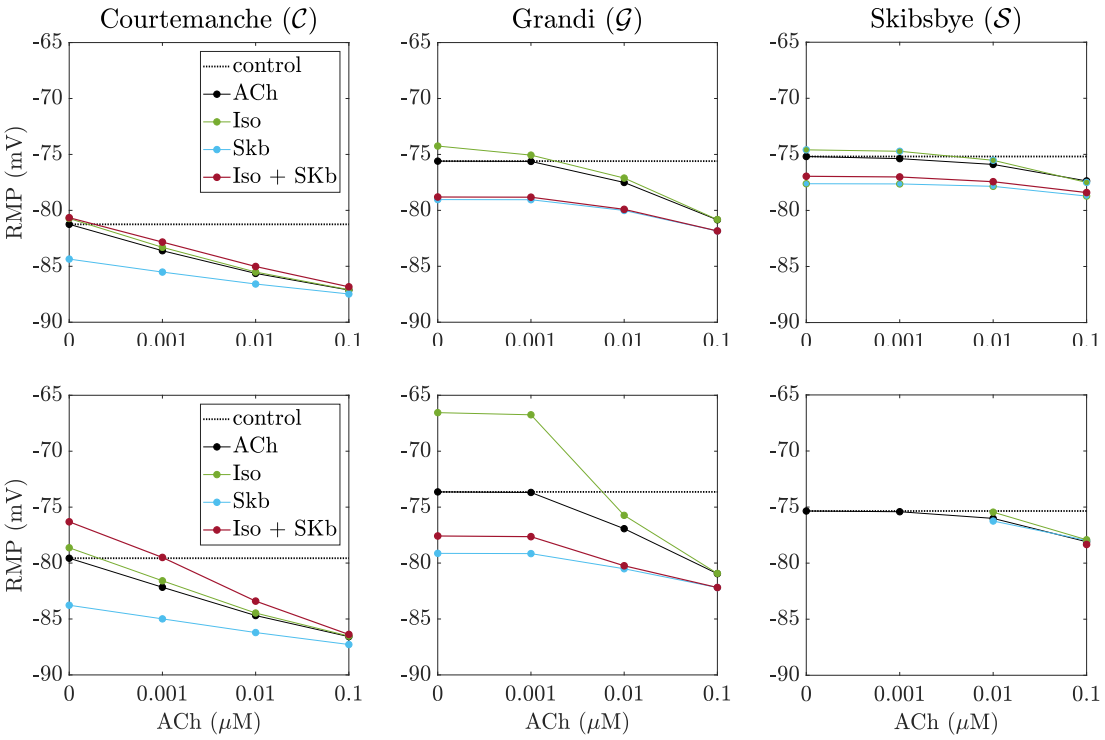

Figure 6S: RMP vs ACh concentration for human atrial cardiomyocytes models paced at a CL of 500 ms (a) and 300 ms (b), at four different tested scenarios comprising cholinergic stimulation individually and in combination with β-adrenergic stimulation and/or SKb.

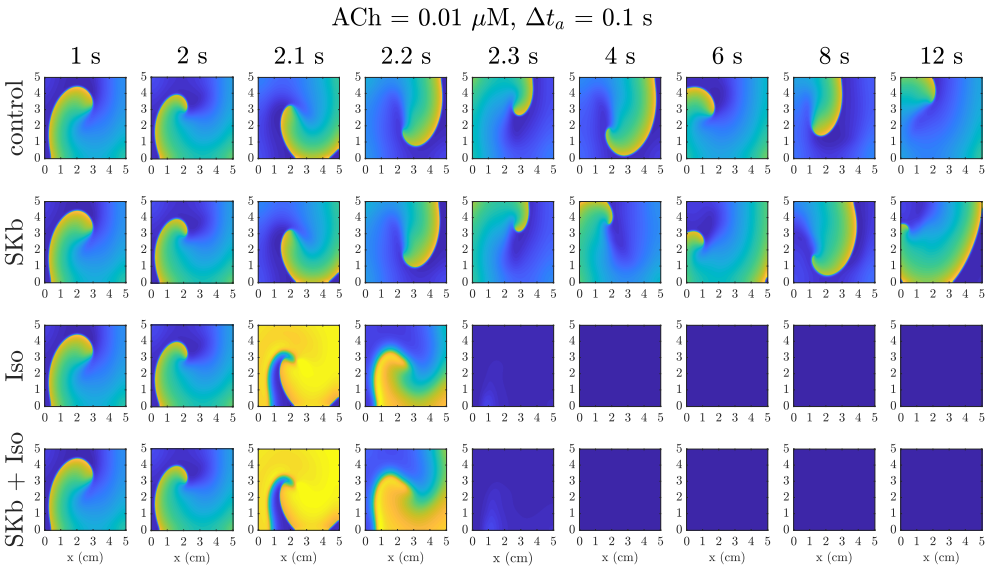

Figure 7S: Voltage maps along time showing rotors in 2D human atrial tissues under 0.01 μM ACh. First row: control, second row: + SKb, third row: + 1 μM Iso, fourth row: + SKb + 1 μM Iso. Iso and/or SKb were applied progressively with Δt_a=0.1 s starting at time = 2 s.

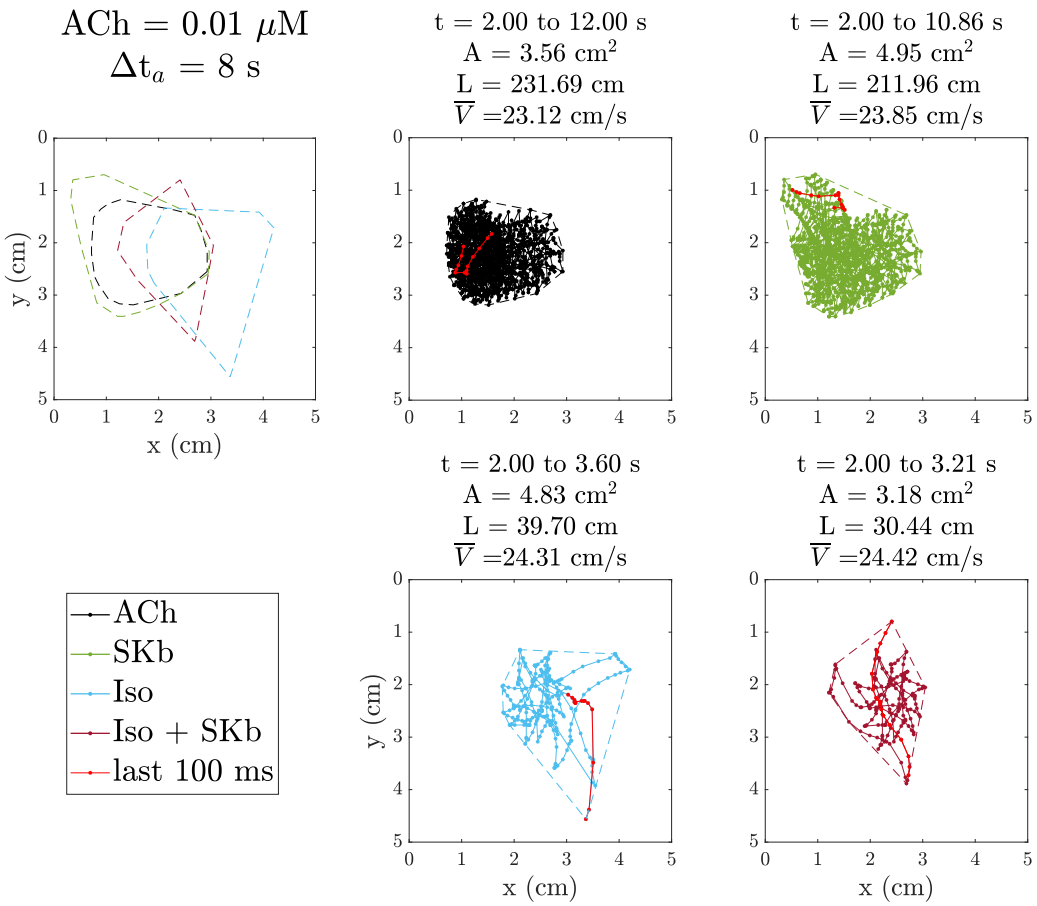

Figure 8S: Rotor tip trajectory characteristics in terms of surface covered by the rotor tip (A), distance covered (L) and mean velocity ($\overline{V}$) when ACh=0.01 μM and Δt_a=8 s. In red the final segment of PSs, corresponding to the last 100 ms, is highlighted to point out the rotor tail. The top left panel represents the comparison between the area covered by the rotors in the different cases. The trajectory is analyzed for the entire lifespan of the rotor.

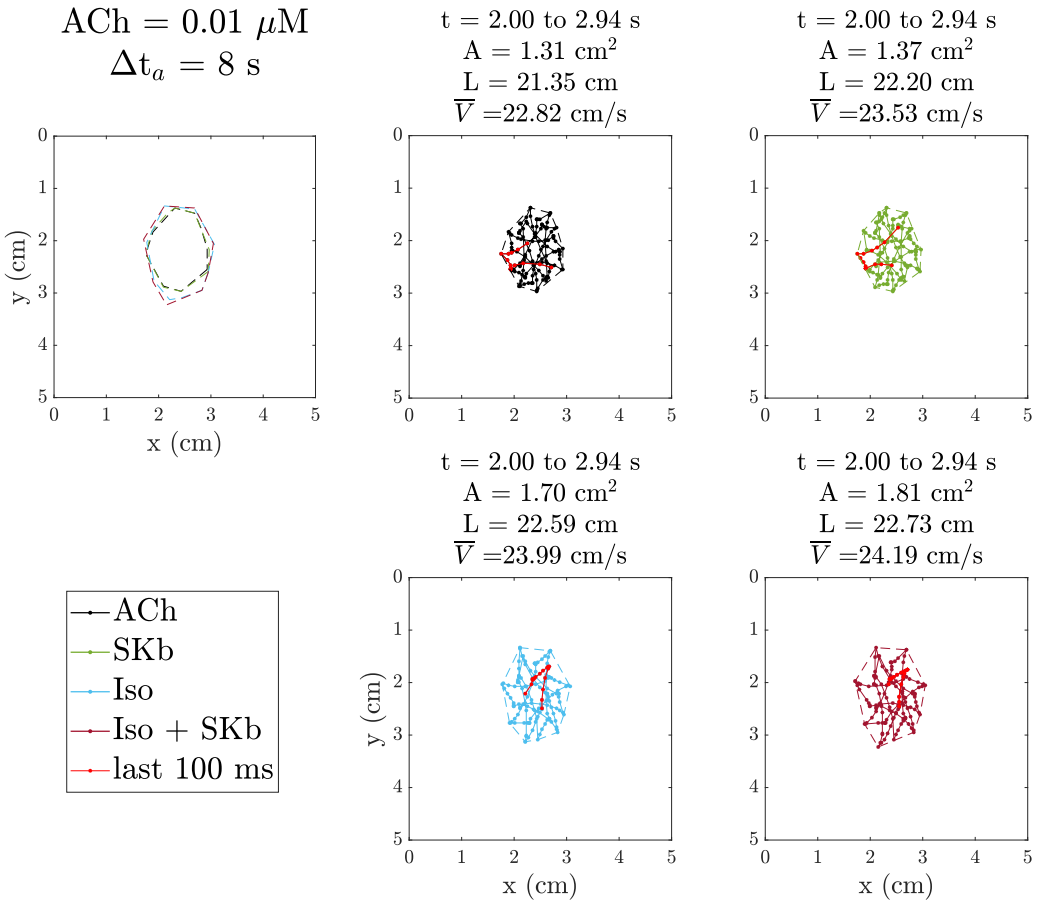

Figure 9S: Rotor tip trajectory characteristics in terms of surface covered by the rotor tip (A), distance covered (L) and mean velocity ($\overline{V}$) when ACh=0.01 μM and Δt_a=8 s. The figure is structured as Fig. 8S. The trajectory is analyzed in the time span before the onset of instability in the case when it manifested itself earlier.

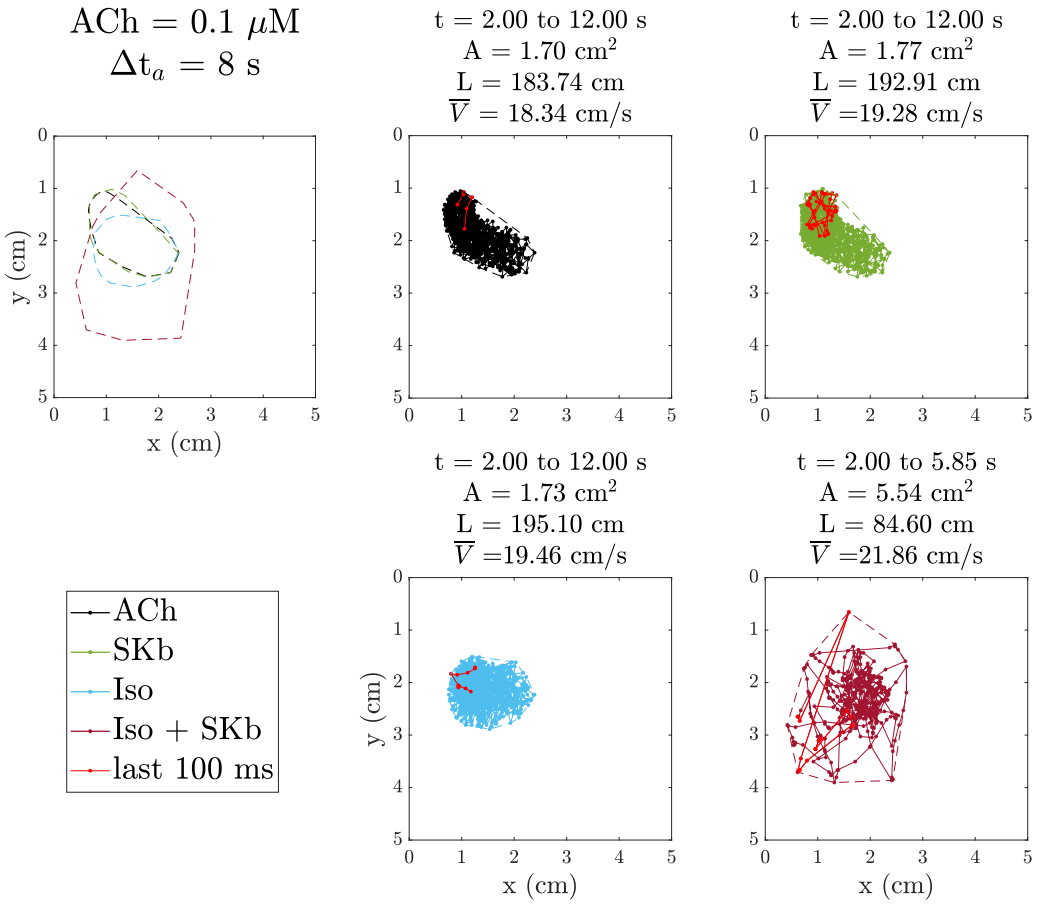

Figure 10S: Rotor tip trajectory characteristics in terms of surface covered by the rotor tip (A), distance covered (L) and velocity ($\overline{V}$) when ACh=0.1 μM and Δt_a=8s. The figure is structured as Fig. 8S. The trajectory is analyzed for the entire lifespan of the rotor.

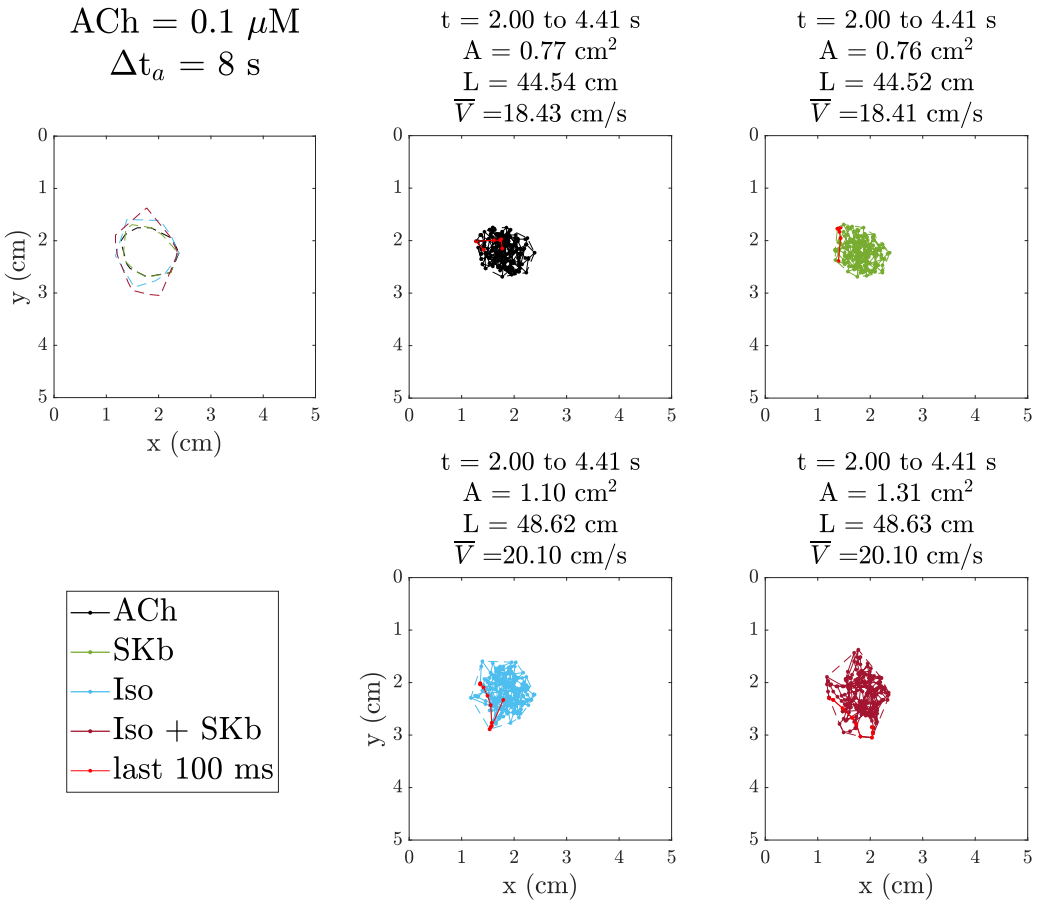

Figure 11S: Rotor tip trajectory characteristics in terms of surface covered by the rotor tip (A), distance covered (L) and mean velocity ($\overline{V}$) when ACh=0.1 μM and Δt_a=8 s. The figure is structured as Fig. 8S. The trajectory is analyzed in the time span before the onset of instability in the case when it manifested itself earlier.

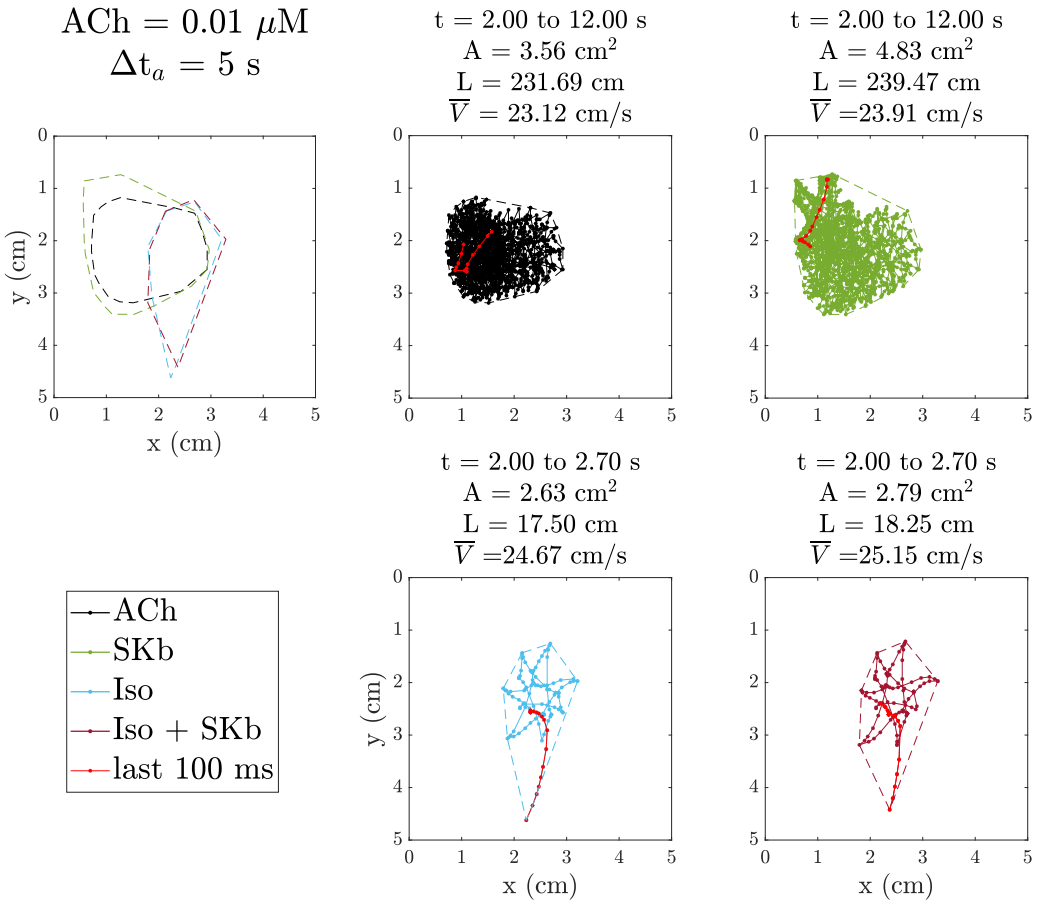

Figure 12S: Rotor tip trajectory characteristics in terms of surface covered by the rotor tip (A), distance covered (L) and mean velocity ($\overline{V}$) when ACh=0.01 μM and Δt_a=5 s. The figure is structured as Fig. 8S. The trajectory is analyzed for the entire lifespan of the rotor.

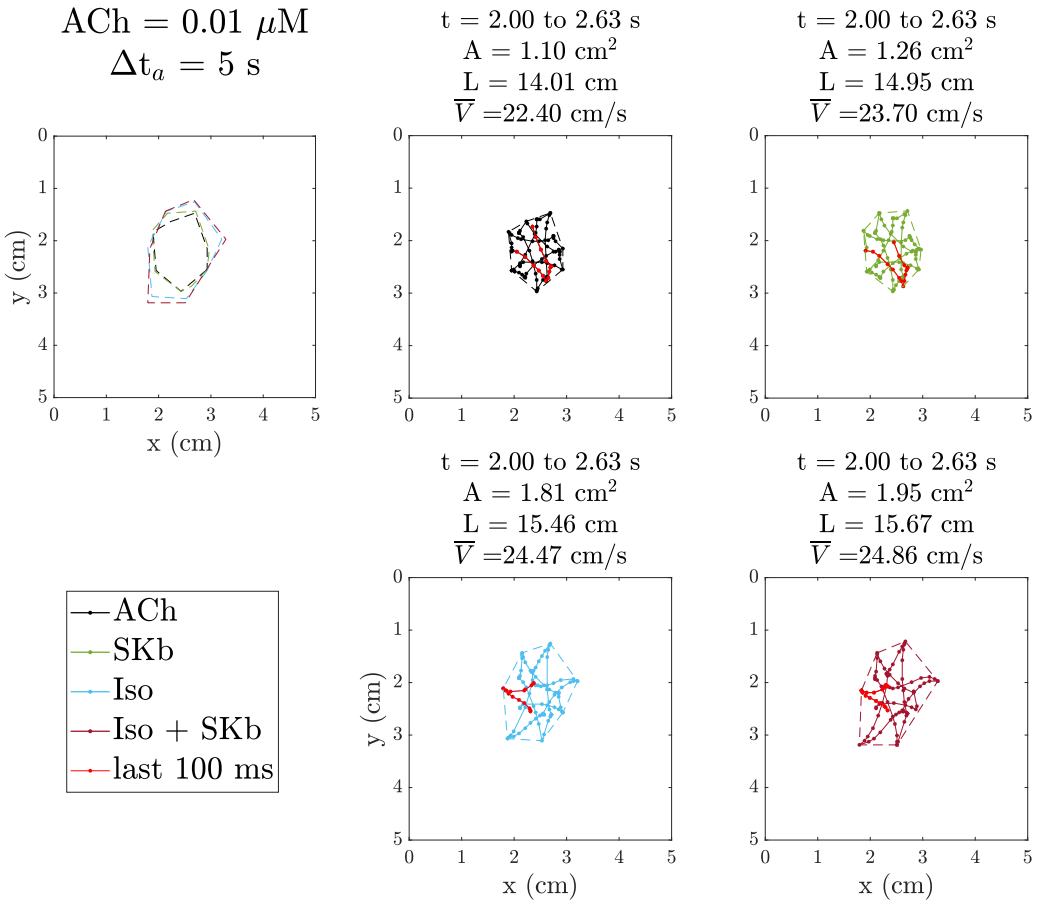

Figure 13S: Rotor tip trajectory characteristics in terms of surface covered by the rotor tip (A), distance covered (L) and mean velocity ($\overline{V}$) when ACh=0.01 μM and Δt_a=5 s. The figure is structured as Fig. 8S. The trajectory is analyzed in the time span before the onset of instability in the case when it manifested itself earlier.

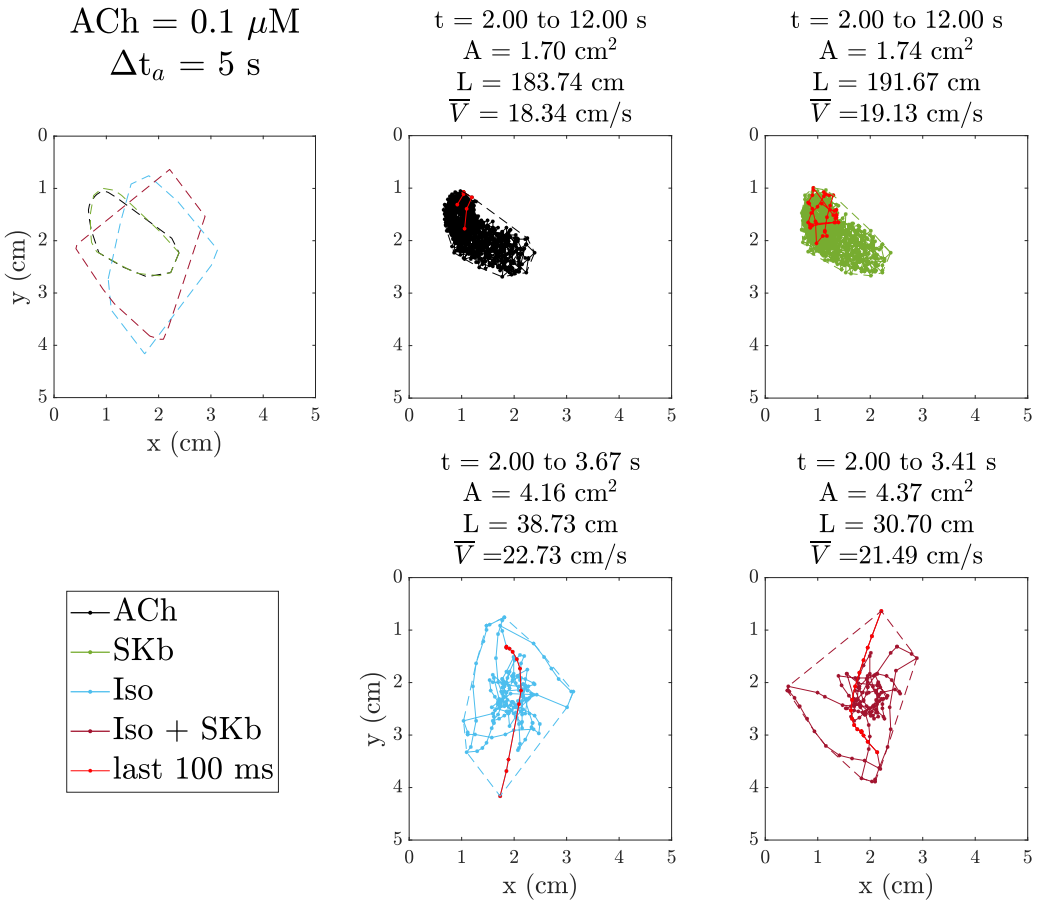

Figure 14S: Rotor tip trajectory characteristics in terms of surface covered by the rotor tip (A), distance covered (L) and mean velocity ($\overline{V}$) when ACh=0.1 μM and Δt_a=5 s. The figure is structured as Fig. 8S. The trajectory is analyzed for the entire lifespan of the rotor.

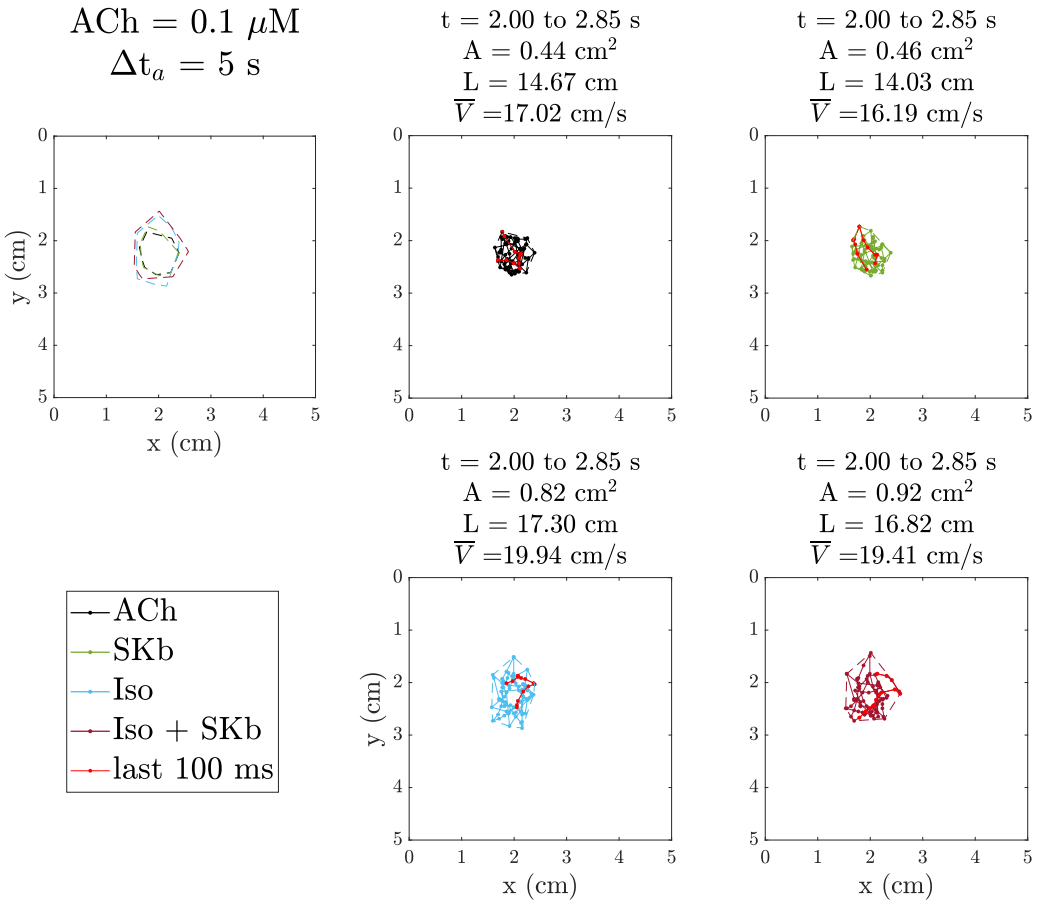

Figure 15S: Rotor tip trajectory characteristics in terms of surface covered by the rotor tip (A), distance covered (L) and mean velocity ($\overline{V}$) when ACh=0.1 μM and Δt_a=5 s. The figure is structured as Fig. 8S. The trajectory is analyzed in the time span before the onset of instability in the case when it manifested itself earlier.

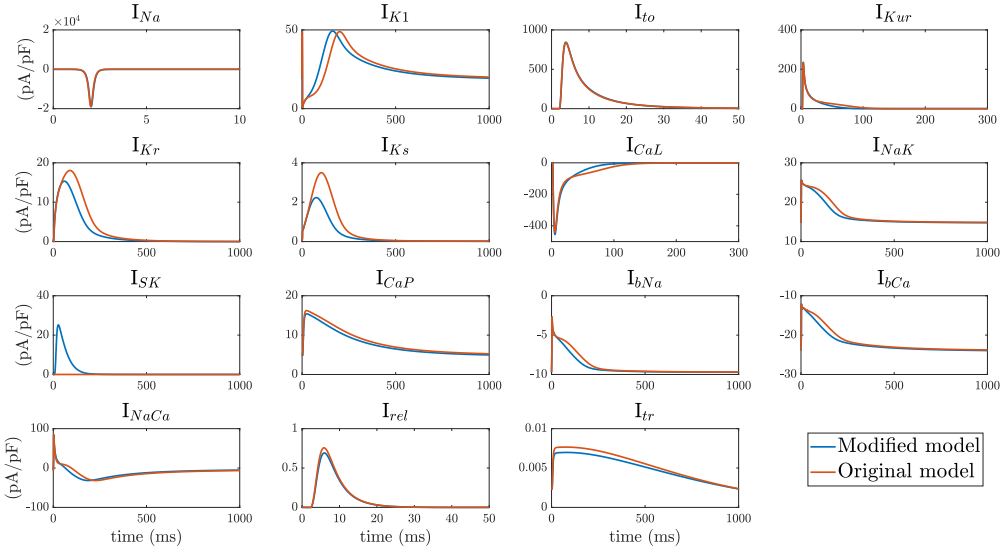

Figure 16S: Representation of the individual currents in the $\mathcal{C}$ model before (red) and after (blue) the introduction of the I_{SK} current.

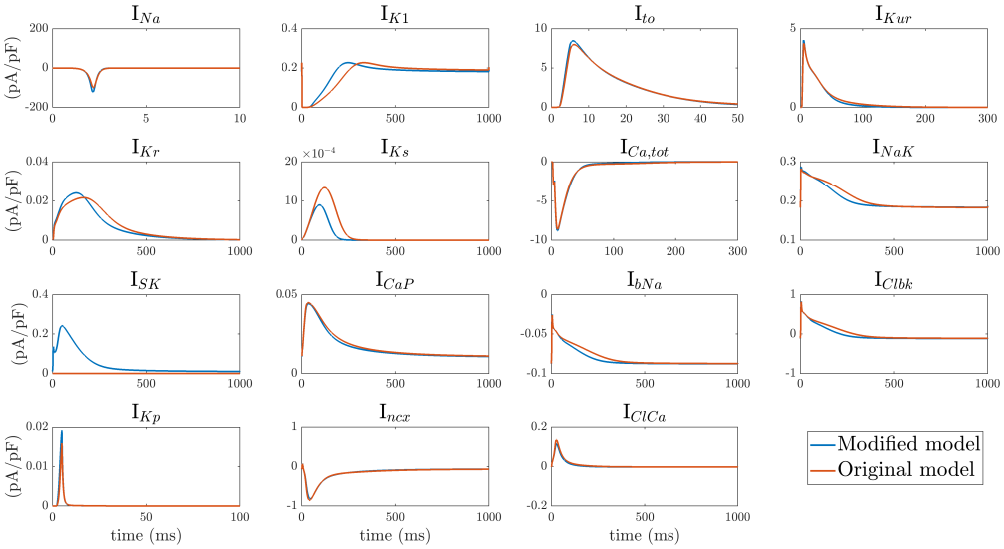

Figure 17S: Representation of the individual currents in the $\mathcal{G}$ model before (red) and after (blue) the introduction of the I_{SK} current.

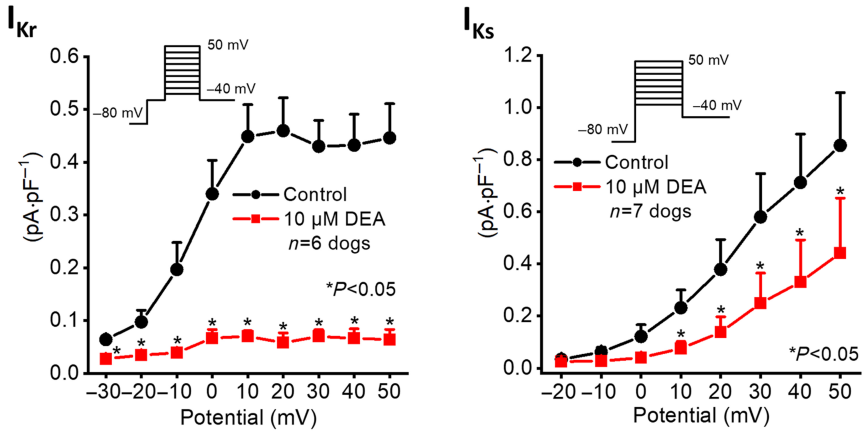

Figure 18S: IV curves for I_{Ks} and I_{Kr} adapted from Kohajda et al. [4]. Values obtained from dog myocytes. Here we are interested in the control black curves representing control conditions.

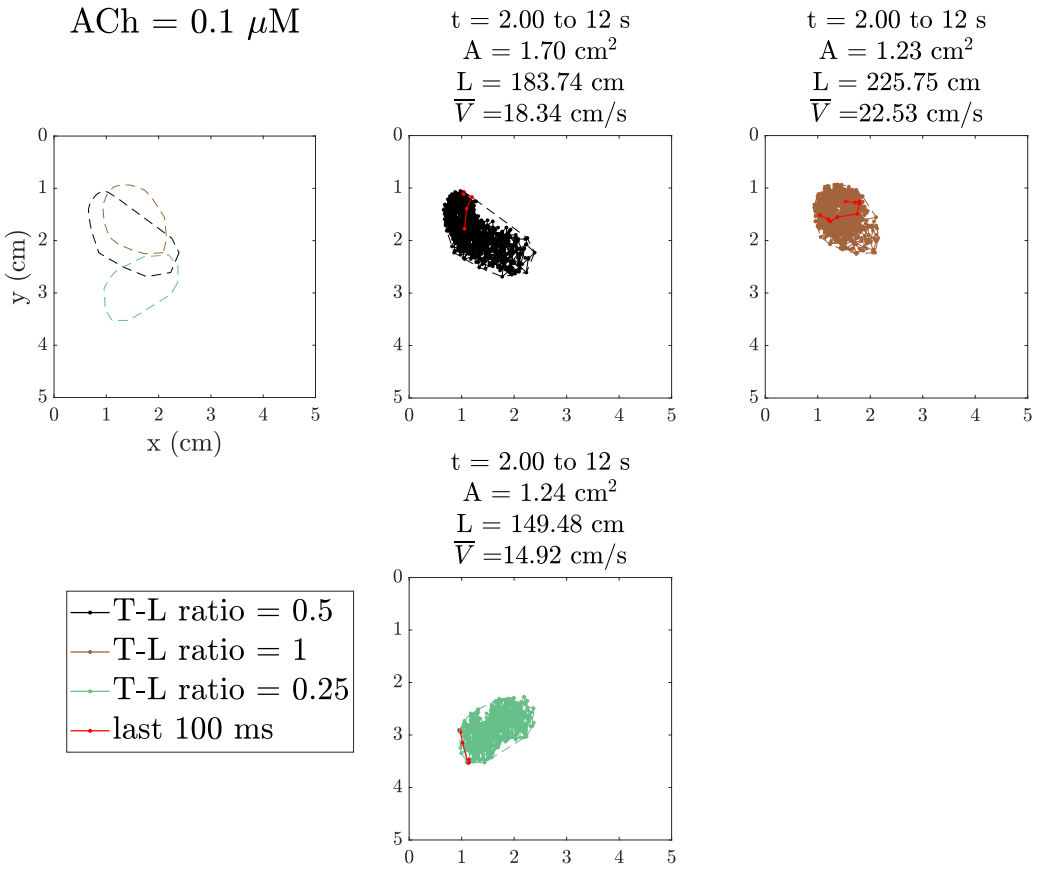

Figure 19S: Effect of different transverse-to-longitudinal ratios (0.25, 0.5, 1) on the following rotor tip trajectory characteristics (ACh = 0.1 μM): surface (A) and distance (L) covered by the rotor tip and mean velocity ($\overline{V}$).